Crystallization of calcium carbonate beneath insoluble monolayers: suitable models of mineral–matrix interactions in biomineralization?

Marc Fricke, Dirk Volkmer

Angaben zur Veröffentlichung / Publication details:

Fricke, Marc, and Dirk Volkmer. 2006. "Crystallization of calcium carbonate beneath insoluble monolayers: suitable models of mineral–matrix interactions in biomineralization?" In *Biomineralization I: crystallization and self-organization process*, edited by Kensuke Naka, 1–41. Berlin [u.a.]: Springer. https://doi.org/10.1007/128_063.

Crystallization of Calcium Carbonate Beneath Insoluble Monolayers: Suitable Models of Mineral–Matrix Interactions in Biomineralization?

Marc Fricke[1,2] · Dirk Volkmer[1]

[1]Anorganische Chemie II, Universität Ulm, Albert-Einstein-Allee 11, 89081 Ulm, Germany
dirk.volkmer@uni-ulm.de

[2]ISIS, groupe BASF, ULP, 8, allée Gaspard Monge, 67083 Strasbourg, France

Abstract The growth of inorganic materials below negatively charged monolayers is frequently considered to be a suitable model system for biomineralization processes. The fact that some monolayers give rise to oriented overgrowth of calcium carbonate crystals has been interpreted in terms of a geometrical and stereochemical complementarity between the arrangement of headgroups in the monolayer and the position of Ca ions in the crystal plane that attaches to the monolayer. However, comparative investigations of the growth of calcium carbonate beneath monolayers of macrocyclic polyacids have demonstrated that non-directional electrostatic parameters, such as the average charge density or the mean dipole moment of the monolayer, determine the orientation and the polymorph of the overgrowing crystals. The results show that it is possible to control the surface charge densities in monolayers by the appropriate design of amphiphilic molecules. A switch in polymorph occurs above a critical monolayer charge density at

which aragonite or vaterite nucleation takes place, presumably via a kinetically controlled precipitation process.

Keywords Calcium carbonate · Biomineralization · Mollusc shell · Nacre · Monolayers · Template mechanism · Epitaxy

1 Introduction

Many organisms have developed sophisticated strategies for directing the growth of the inorganic constituents of their mineralized tissues. Active control mechanisms are effective at almost all levels of structural hierarchy, ranging from the nanoscopic regime (the nucleation of a crystallite at a specific site) up to the macroscopic regime, where the biophysical properties of the mineralized tissue are matched to certain functions [1]. Among the many open questions, one of the most challenging scientific problems is to gain greater insight into the molecular interactions occurring at the interface between the inorganic mineral and the macromolecular organic matrix. Biogenic crystals often express exceptional habits that are seemingly unrelated to the morphology of the same type of crystals grown under equilibrium conditions.

The morphology of the calcified tissue is ultimately encoded in the genome governing the biosynthesis of required materials at the cellular level of structural hierarchy. Therefore, biomineralization, as a highly complex phenomenon involving living organisms, cannot be reduced to a single mechanistic aspect (Fig. 1). The following representation of $CaCO_3$ mineralization in molluscs, and its mimesis by simple model systems, is admittedly a crude simplification that concentrates mainly on structural aspects, while at the same time ignoring the dynamic character of the biological process. Special emphasis here is placed on $CaCO_3$ crystal nucleation, i.e., the early stages of crystal growth where the system properties might be described by (supra-)molecular recognition events occurring at the mineral–matrix interface. At this level, a common feature seems to exist for many mineralizing organisms: the interaction of highly specialized acidic macromolecules with different surfaces of the growing single crystal [4, 5]. For the most widespread calcified tissues it is frequently assumed that a structurally rigid composite matrix consisting of fibrous proteins and acidic macromolecules adsorbed thereon acts as a “supramolecular blueprint” that templates nucleation of the inorganic phase. Subsequent crystal growth proceeds within a specialized compartment enclosing a suitable aqueous microenvironment. The particular composition of solutes, which is often comprised of a complex mixture of dissolved electrolytes and macromolecules, has a strong influence on the morphology of the crystals. In the course of mineral deposition, growth mod-

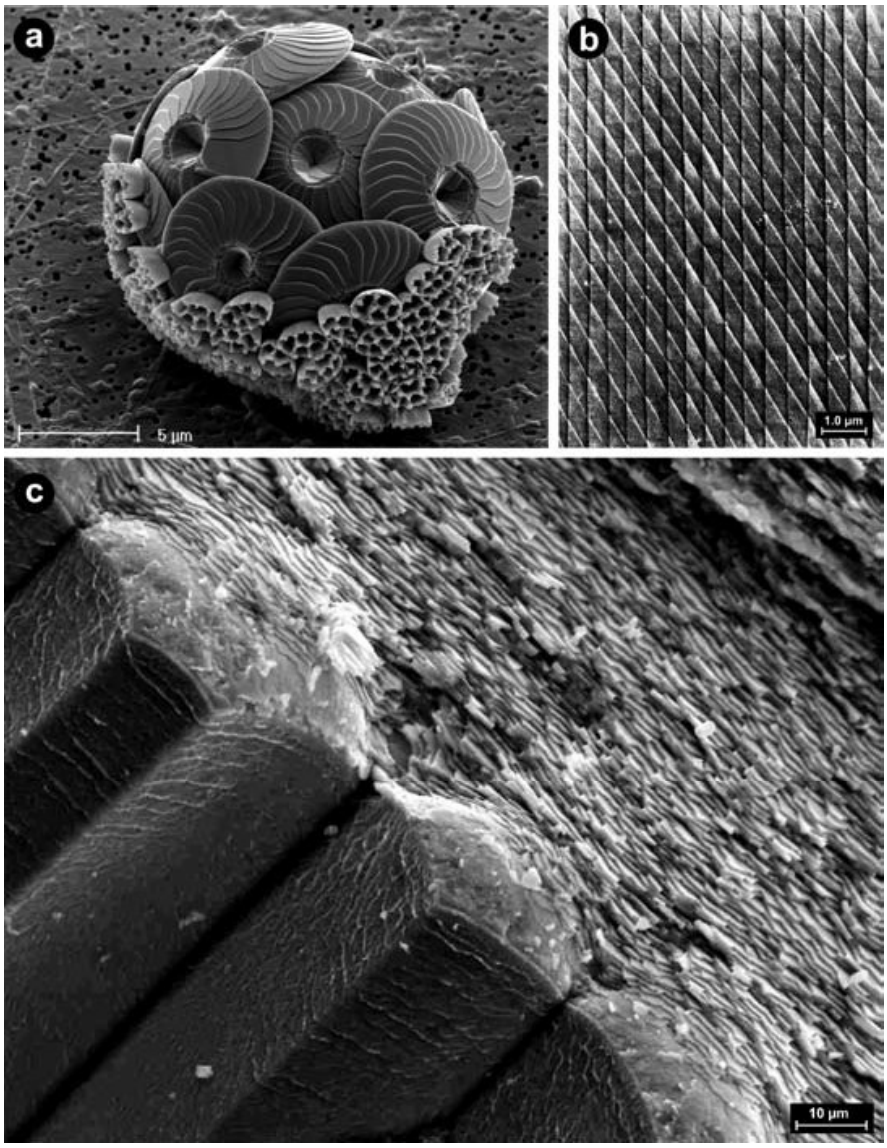

Fig. 1 Examples of biologically produced highly oriented calcerous structures exemplifying the astonishing degree of sophistication with which certain organisms can control the growth of inorganic crystals. **a** SEM of the calcerous test ("coccosphere") produced by a coccolithophorid, a unicellular marine photosynthetic alga. Note the interlocked arrangement of minute calcite plates that cover the cell. Shown here is a combination coccosphere with both hetero- and holococcoliths (*Calcidiscus leptoporus* & *Syracolithus quadriperforatus*). Combination coccospheres are thought to represent a transitional state between heterococcolithophorid and holococcolithophorid phases of the life cycle [2]. (Micrograph courtesy of J. Young, Natural History Museum, London and M. Geisen, AWI Bremerhaven). **b** Freshly fractured shell of a Devonian brachiopod (*Pholidostrophia nacrea*) showing a crisscrossed pattern of calcite crystals that acts as a natural optical diffraction grating. This pattern gives rise to a nacreous luster and pearly iridescence that is unusual for calcite [3]. (Single-stage platinum-carbon replica. Approximately 20 000×. TEM photo courtesy of K.M. Towe, Smithsonian Institution). **c** SEM of a fractured shell of *Anodonta cygnea* showing the transition from the prismatic to the nacreous layer (prisms *bottom*, nacre *top*). Note that in this species both morphologically distinct layers consist of aragonite, whereas in most mollusc shells the prisms are normally made of calcite. (Micrograph courtesy of F. Marin, Université de Bourgogne)

ifiers may interact with the maturing crystal in different ways: dissolved macromolecules may be adsorbed onto specific crystal faces, thus slowing down or inhibiting deposition rates along certain crystallographic directions. Adsorbed macromolecules may be completely overgrown by the mineral to produce lattice defects or to introduce discontinuities in the crystal texture. Current research efforts of biologists and biochemists are focused on the isolation and characterization of macromolecules from calcified tissues, and the functional properties of isolated macromolecules or fractions of macromolecules are systematically investigated regarding their ability to influence $CaCO_3$ nucleation, growth, and polymorphism. Biologically inspired synthetic strategies attempt to assemble artificial matrices in order to mimic structural and functional properties of mineralizing tissues.

Special emphasis in this review is laid upon the crystallization of calcium carbonate underneath insoluble monolayers – a model system that is often regarded as a straight-forward experimental approach toward biomimetic crystallization. A summary of the most important experimental data gained from such monolayer investigations is presented here, with particular emphasis placed on our own work in this field. As will be shown, the numerous enthusiastic early reports of epitaxial growth of inorganic crystals beneath membrane-like monolayers might require some profound revision of the suggested mechanisms. Evidence from recent investigations suggests that the commonly held view of a structure-directing organic template matrix represents an oversimplified concept of the complex crystallization process. The current debate on the various roles of amorphous inorganic precursors, which were recently identified in biological specimen and biomimetic crystallization assays, reflects the many contradictory experimental findings and statements concerning this topic. An updated view on the putative crystallization stages taking place at the mineral/organic matrix interface is presented in the final chapter, which highlights the dynamic cooperative character of the process.

2
Crystallochemical Aspects of $CaCO_3$ Biomineralization

$CaCO_3$, together with amorphous silica, is the most abundant biomineral. There exist three $CaCO_3$ polymorphs – *calcite*, *aragonite*, and *vaterite* – all of which occur in calcified tissues. A monohydrate (*monohydrocalcite*) and a hexahydrate form (*ikaite*) of $CaCO_3$ have been characterized as metastable precursor phases during the incipient stages of crystal formation (Table 1).

At ambient conditions, calcite is the thermodynamically most stable $CaCO_3$ polymorph. However, from supersaturated aqueous solutions containing Mg^{2+} at a molar ratio Mg/Ca > 4 (comparable to the composition of seawater), the only observed crystalline phase is aragonite, while at high su-

Table 1 Characteristics of the most important $CaCO_3$ mineral phases

Mineral (formula)	Crystal system (space group)	Spec. density [g/cm^3]	Solubility [$-\log K_{sp}$]	Biologic occurrence	Crystal data ref.
Calcite ($CaCO_3$)	Trigonal ($R\bar{3}c$)	2.71	8.48	Very common	[6]
Aragonite ($CaCO_3$)	Orthorhombic ($Pmcn$)	2.93	8.34	Very common	[7]
Vaterite ($CaCO_3$)	Hexagonal ($P6_3/mmc$)	2.54	7.91	Rare	[8]
Monohydrocalcite ($CaCO_3 \cdot H_2O$)	Trigonal ($P3_121$)	2.43	7.60	Very rare	[9]
Ikaite ($CaCO_3 \cdot 6H_2O$)	Monoclinic ($C2/c$)	1.77	7.12	Unknown	[10]

Data adapted in part from [11]

persaturation the metastable polymorph vaterite precipitates from solution. The arrangement of the ions in crystalline $CaCO_3$ can be described in terms of separate layers of cations and anions. Coordination environments for Ca^{2+} ions (CO_3^{2-}, respectively) in the polymorphs differ from each other, as a result of different successions of layers, as well as different crystallographic orientations of the planar carbonate groups in the crystal lattices (Fig. 2). In calcite, each single densely packed Ca layer parallel to the *ab* plane is situated between single layers of CO_3^{2-}, with each layer containing anions oriented in opposite directions. Each Ca^{2+} ion is situated in a distorted octahedral coordination environment of six CO_3^{2-} anions. In aragonite, the positions of the

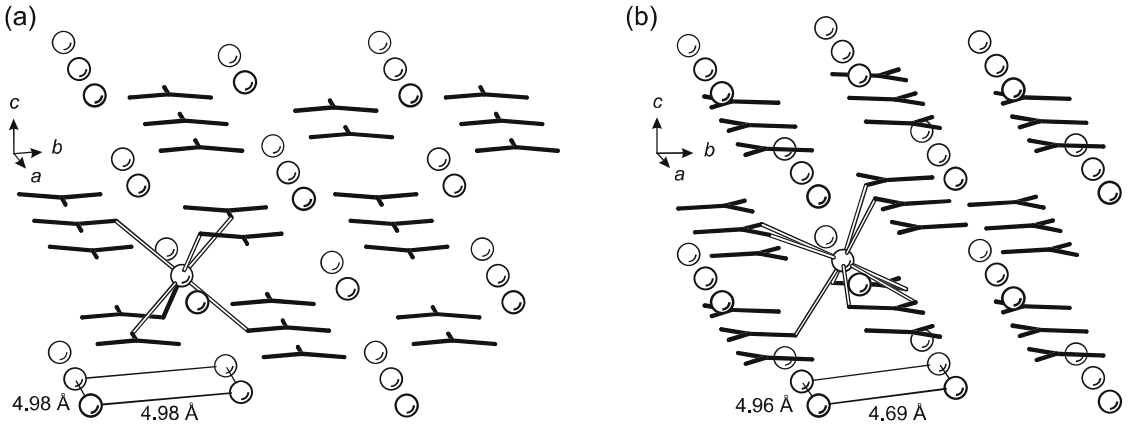

Fig. 2 Ion packing arrangement in the crystal structures of **a** calcite and **b** aragonite. The coordinative bonds between CO_3^{2-} anions (*black sticks*) and one of the Ca^{2+} ions (*open circles*) are emphasized with *open lines*. The minimum distances of Ca^{2+} ions in the *ab* planes for both crystal lattices are indicated at the *bottom*. (Reprinted from [18] with permission)

Ca^{2+} ions in the *ab* plane are nearly identical to those in the calcite structure. In contrast, the CO_3^{2-} anions below and above the Ca layer are separated into two layers, which are lifted by 0.98 Å along the *c* direction, leading to an overall ninefold coordination of Ca^{2+} ions [12].

Single crystals (regardless of crystal system, space group symmetry, and chemical composition) are intrinsically anisotropic, that is, most physical properties depend strongly on direction. For ionic crystals, such as calcium carbonate, this leads to a pronounced brittleness and cleavability along special directions of the crystal lattice. Typical cleavage planes of calcite are the six symmetry equivalent {10.4} crystal faces of the trigonal lattice, which leads to the rhombohedral shape of single crystals grown from supersaturated solution. The primary reason for the high stability and easy cleavage of the {10.4} crystal faces of calcite is that they consist of a close-packed, non-polar arrangement of calcium and carbonate ions (Fig. 3). In contrast, many low-index cleavage planes of the calcite lattice (such as (00.1) or (01.2)) represent

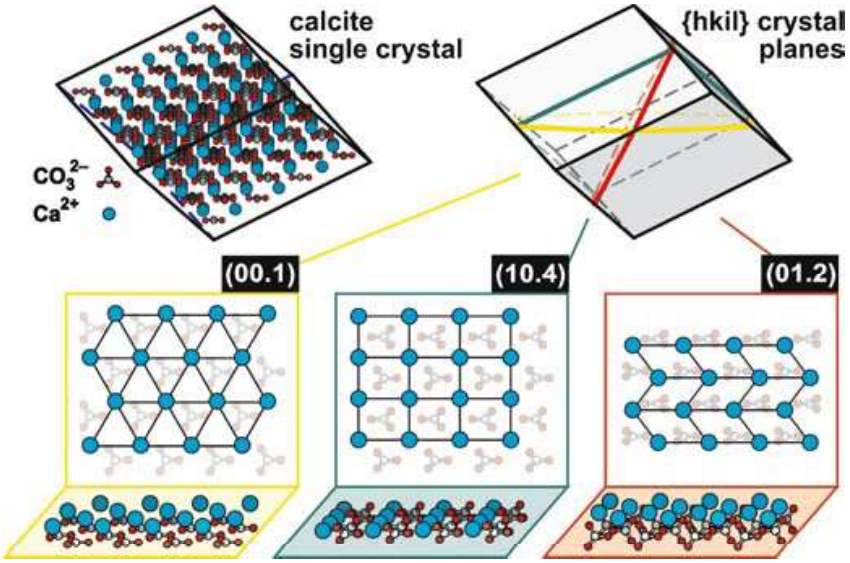

Fig. 3 Crystal planes resulting from cutting a calcite single crystal along different crystallographic directions. Calcite crystallographic indices are presented in the Miller–Bravais four-index system *hkil* for planes and faces. The graphical schemes are based on the hexagonal unit cell for calcite (unit cell parameters: $a = 4.989$ Å, $c = 17.062$ Å). The displayed shape of the calcite crystal corresponds to its {10.4} crystal form, i.e., the single crystal is enclosed by a set of symmetry-equivalent {10.4} crystal faces. Note that for the trigonal crystal system of calcite, four-membered ("Miller–Bravais") indices of the common form {*hkil*} are frequently used, however the index "i" is redundant and can be calculated from h+k+i = 0 or i = –(h+k). Therefore, in the literature the fourth index i is often omitted or symbolized by a dot. *Lower part*: Three different cleavage planes of the calcite crystal lattice are shown. Note that the resulting 2-D tilings differ by their plane crystallographic ("wallpaper symmetry") groups, of which a total of 17 exist. Another distinction is the separation of ionic groups into different layers. Cleaving a calcite crystal along (00.1) or (01.2), as opposed to (01.4), leads to the formation of highly polar crystal faces, which are energetically unfavorable

highly polar crystal faces, that is, each sort of ion is situated in a separate layer, leading to a macroscopic dipole moment. Polar crystal faces are normally not expressed in the equilibrium growth form of crystals. However, crystal growth from strongly polar solvents or the presence of (charged) inhibitors may result in slowing down the growth rate in a particular direction.

Since a cleavage plane of an ionic crystal is uniquely defined by its plane crystallographic symmetry and its polarity, it should in principle be possible to define a kind of "blueprint", i.e., a planar arrangement of ions or molecules that perfectly mirrors the geometrical and stereochemical properties of the mineral surface. If the developing single crystals grow totally co-aligned with respect to oriented domains of the organic matrix, the growth process is termed heteroepitaxy. As illustrated in Fig. 4, different epitaxial growth modes are distinguishable, depending on the structural similarity of the substrate and its overgrowing phase.

Layer-by-layer growth (*Frank van der Merwe* mode) is typically observed if a strict epitaxial relationship exists between the overgrowing film and the substrate. Island (*Volmer–Weber*) growth is observed when the attraction between molecules of the film is stronger than that between the film and the substrate, such that the film tends to coalesce as 3-D islands rather than wetting the substrate. An intermediate case between these two growth modes is also encountered – *Stranski–Krastanov* growth – which is described by the initial formation of a film layer followed by island growth on that layer. This can result if there is a slight lattice mismatch, but still favorable interaction, between the film and substrate [14].

If calcifying organisms were able to produce such "blueprints", and to expose them at defined sites of their soft tissues, inorganic crystals would be expected to grow epitaxially there, much as they do on inorganic substrates providing similar lattice constants and surface energies. This *Ansatz* represents in short the commonly held view of templated or epitaxial crystal growth as a fundamental characteristic of many biomineralizing organisms. In fact, some (but not all) calcifying organisms are able to produce highly organized crystal architectures with an astonishing degree of perfection (some prominent examples are shown in Fig. 1). However, the occurrence of highly regular and oriented biogenic crystal textures does not *automatically* imply

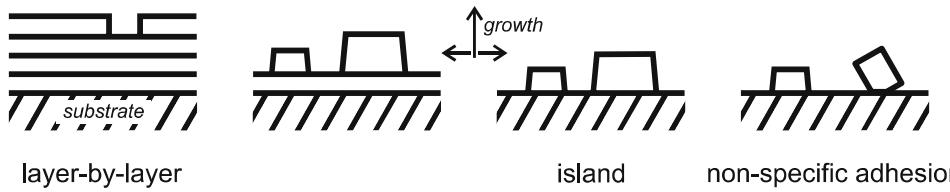

Fig. 4 Schematic representation of different epitaxial growth modes. The 3-D alignment of the over-growing phase relative to the substrate is primarily dependent on the matching of the two different lattices. The structural similarity is most pronounced in the layer-by-layer growth mode. (Adapted from [13])

the validity of epitaxy as a control mechanism involved in biomineral formation, since there are many periodic tilings and patterns in nature made of organic (macromolecular and cellular) materials (e.g., epithelial surface reliefs and color patterns) [15, 16], that can hardly be presumed to form by virtue of epitaxy.

In fact there are many puzzling details of the growth characteristics of biogenic crystals that cannot be explained by epitaxy models, i.e., by a structural commensurability between the organic template surface and the overgrowing crystals. Some of these contradictory facts will be discussed in the following chapters.

3
Mollusc Shell Formation

Molluscs, which are among the most thoroughly investigated organisms in biomineralization studies, build concrete shells from $CaCO_3$ [17]. The mollusc shell may be regarded as a microlaminate composite consisting of layers of highly oriented $CaCO_3$ crystals interspersed with thin sheets of an organic matrix. Crystals within separate shell layers usually consist of either pure aragonite or pure calcite. Vaterite, when present, is usually associated with shell repair. Shell formation occurs in two principal phases. The first involves the cellular processes of ion transport and organic matrix synthesis, which occur in different compartments of the molluscan mineralizing system. The second phase consists of a series of crystal nucleation and growth processes taking place in a specialized mineralization compartment, the *extrapallial space* (Fig. 5, left) [18].

In the past, special attention has been paid to the microstructure of nacre (the iridescent inner layer of mollusc shells) which exhibits an exceptionally regular arrangement of tabular aragonite crystals (Fig. 5, right). In order to grow crystals into a highly regular brickwork-like pattern, numerous nucleation events would have to be synchronized to each other at distant locations. An alternative growth mechanism was proposed recently to explain the precision by which aragonite platelets are uniformly co-aligned within the same and consecutive layers. According to this model, nacre may be assembled from extended, continuous single-crystalline domains of aragonite platelets that are interconnected by mineral bridges through perforated sheets of an organic matrix [19].

Considered as a whole, the physiological processes that ultimately lead to the formation of a complete mineralized mollusc shell are largely unknown. However, the general consensus is that the crystal nucleation and growth events are strictly regulated by a number of highly specialized organic macromolecules. Unfortunately, a deeper understanding of the biomineralization processes at the molecular level of structural hierarchy is hampered by our

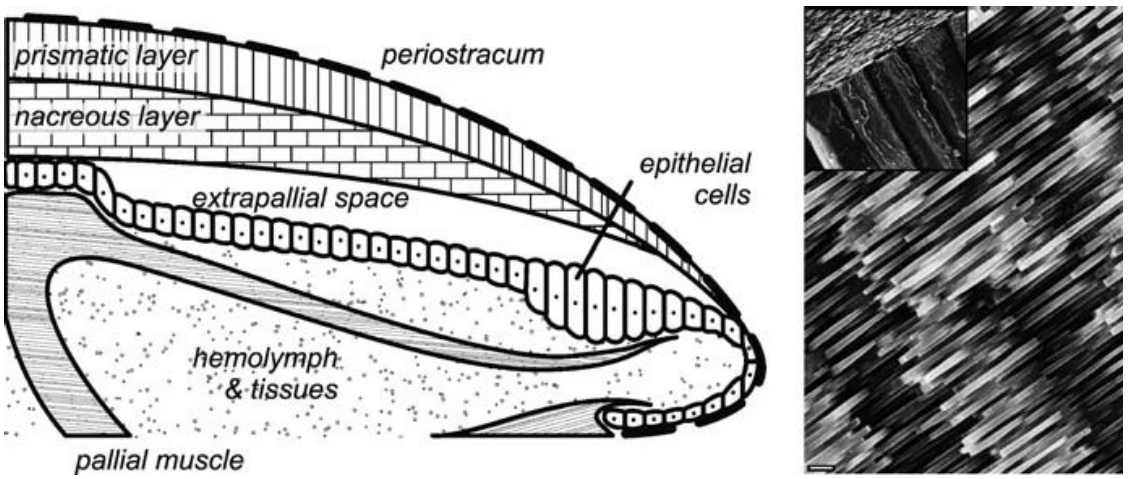

Fig. 5 *Left*: Transverse section of the mantle edge of a bivalve showing the system of compartments. *Right*: Fractured surface of the nacreous layer of the bivalve mollusc *Atrina rigida*. The *inset* shows the inner nacreous layer of tabular aragonite crystals (*top*) and the outer prismatic layer of columnar calcite crystals (*bottom*). (SEM micrographs, *scale bar* denotes 1 μm). Note that the particular crystal morphologies in different layers are not stringently linked to a single $CaCO_3$ polymorph: some organisms build up crystal textures similar to nacre (so-called semi-nacre) from calcite instead of aragonite, whereas others deposit a prismatic layer consisting entirely of aragonite (Fig. 1). (Reprinted from [18] with permission)

lack of knowledge of the 3-D structures of macromolecules that are directly associated with the mineral layer.

A recent literature search yielded very few examples in which complete or partial information about the *primary* structure of the macromolecules directly involved in mineralization was obtained (Tables 2 and 3). Traditionally, macromolecules isolated from mollusc tissues have been distinguished into two different classes based on solubility properties [20]. Chemical analysis showed that the water-insoluble fraction consists mainly of fibrous proteins (collagen, chitin) and/or polysaccharides. These macromolecules together build a rigid framework upon which specific macromolecules from the soluble fraction may become adsorbed. The primary function of the insoluble organic matrix is to subdivide the mineralization compartment into an organized network of microcompartments and thus to delimit the available space for crystal growth and/or to constrain the crystal packing arrangement to a certain extent. The surface of this macromolecular assembly may serve as a supramolecular template for oriented nucleation of single crystals, and in fact crystallization experiments employing reconstructed matrices of purified mollusc shell macromolecules have shown that it is possible to switch between different $CaCO_3$ polymorphs [21, 22] and to rebuild in vitro the gross structural features of the nacreous layer [23].

The macromolecules present in the soluble fraction share common sequence motifs consisting of repeating oligomeric units of acidic residues.

Table 2 Summary of *water-insoluble* proteins isolated from mollusc shells

Name	Source	Characteristic sequence motif	Associated mineral	Proposed function	Refs.
MSI60	Pearl oyster protein from the nacrous layer	[$Ala_{9–13}$] and [$Gly_{3–15}$]	Aragonite	Framework protein, binding of *Asp*-rich soluble glycoproteins	[24]
MSI31	Pearl oyster protein from the prismatic layer	[$Gly_{3–5}$] and [*Glu*–Ser–*Glu*–*Glu*–*Asp*–X], (X = Thr or Met)	Calcite	Framework protein, binding of *Asp*-rich soluble glycoproteins	[24]
MSI7	Pearl oyster protein from the epithelia of the mantle	[$Gly_{x–y}$]	Aragonite Calcite	Framework protein, acceleration of nucleation and precipitation of $CaCO_3$	[25]
N14, N66	Pearl oyster protein from the nacreous layer	$[Asn–Gly]_{12}$ and $[Asn–Gly]_{57}$	Aragonite	Carbonic anhydrase (N66)	[26]
N16	Pearl oyster protein from the nacreous layer	$[Asn–Gly]_6$ (as well as 4 acidic domains)	Aragonite	Control of crystal growth and morphology	[23]
Lustrin A	Abalone protein from the nacreous layer	[Gly–Ser–Ser–Ser] and [Gly–Ser] (as well as one basic domain)	Aragonite	Adhesion protein	[27]
Prismalin-14	Pearl oyster protein from the prismatic layer	[*Asp*]- and [Gly/Tyr]-rich domains [Pro–Ile–Tyr–Arg] repeats	Calcite	Framework protein	[28]

Table 3 Summary of *water-soluble* proteins isolated from mollusc shells

Name	Source	Characteristic sequence motif	Associated mineral	Proposed function	Refs.
MSP-1	Scallop shell glycoprotein from the foliated layer	[*Asp*–Gly–Ser–*Asp*] and [*Asp*–Ser–*Asp*]	Calcite	Induction of crystal nucleation, control of $CaCO_3$ polymorphism	[29]
Nacrein	Pearl oyster protein from the nacreous layer	[Gly–*X*–Asn], (*X* = *Glu*, Asn, or *Asp*)	Aragonite	Carbonic anhydrase, Ca-binding	[30]
Mucoperlin	Fan mussel protein from the nacreous layer	Tandem repeats rich in [Pro], [Ser] and [Thr]	Aragonite	Induction of crystal nucleation, control of $CaCO_3$ polymorphism	[31]
Perlucin	Abalone protein from the nacreous layer	C-type lectin domains	Aragonite	Glycoprotein receptor	[32]
Perlustrin	Abalone protein	[Cys–X–Cys–Cys–X–X–Cys]	Aragonite	Insulin-like growth factor binding protein	[33]
Aspein	Pearl oyster highly acidic protein from the prismatic layer	[$Asp_{2–10}$] punctuated with [Ser–Gly] dipeptides	Calcite	Control of $CaCO_3$ polymorphism	[34]
AP7 ***AP8*** ***AP24***	Abalone protein from the nacreous layer	[*Asp*–*Asp*] [*Asp*]-rich [*Asp*–*Asp*–*Asp*–*Glu*–*Asp*]	Aragonite	Control of $CaCO_3$ polymorphism	[35, 36]
Calprismin	Fan mussel protein from the prismatic layer	[*Asp*]-rich [Pro]- and [Thr]-rich	Calcite	Cell signalling, matrix-cell interactions	[37]
Caspartin	Fan mussel protein from the prismatic layer	[Asp_{75}]	Calcite	Control of $CaCO_3$ prism formation	[37]
Asprich 1–3	Bivalve proteins from the prismatic layer	[*Asp*]-rich [*Asp*–Glu–Ala–*Asp*]	Calcite	Control of $CaCO_3$ prism formation	[38]

Table 3 contains the available data of fully characterized water-soluble proteins isolated from morphologically different locations of calcified mollusc tissues. However, the heterogeneity of sources/organisms for isolating these macromolecules, their different chemical natures, and their association with different mineral phases clearly rule out a uniform function.

For the induction of calcite and aragonite nucleation, systematic investigations on biological and suitably assembled artificial systems have shed some light on the structural requirements of a putative nucleation site, especially in mollusc shells [39–41]. The model proposes the existence of structurally pre-organized domains of acidic residues, which could serve as a supramolecular template for oriented crystal nucleation. Such highly ordered domains could result from acidic macromolecules being adsorbed on a rigid scaffold of insoluble matrix proteins (Fig. 6).

In fact, investigations of demineralized mollusc shells have shown that the interlamellar organic sheets of nacre consist of thin layers of β-chitin (β-chitin is a water-insoluble $(1 \rightarrow 4)$-linked 2-acetamido-2-deoxy β-D-glucan) [42] sandwiched between thicker layers of silk fibroin-like proteins (Table 2) [43]. Silk fibroin itself possesses microcrystalline domains of repeating $[Gly–Ala–Gly–Ala–Gly–Ser]_n$ units that adopt an antiparallel β-pleated sheet conformation. These domains have a highly regular and hydrophobic surface upon which acidic macromolecules are adsorbed from solution. In the course of adsorption, the acidic macromolecule must fold into the appropriate conformation in order to maximize its hydrophobic interactions with the silk fibroin surface. Possible candidates for acidic macromolecules that

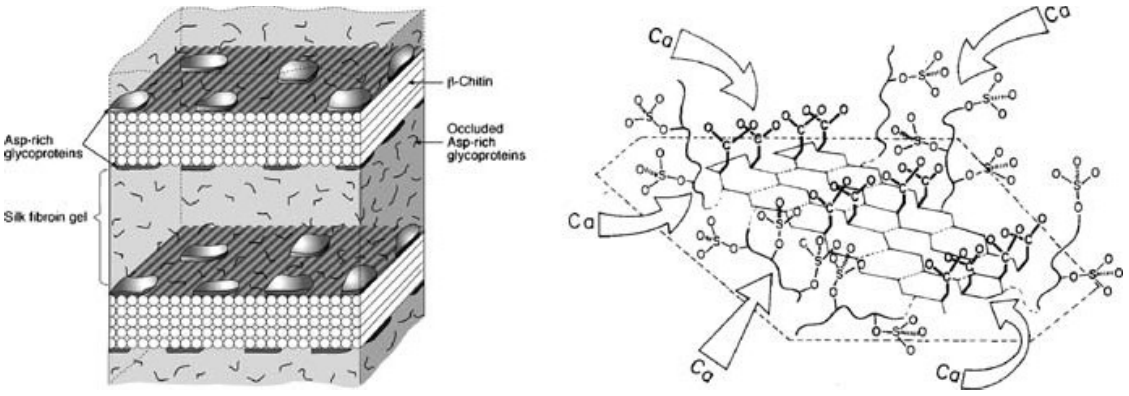

Fig. 6 *Left*: Schematic representation of the organic matrix in the nacreous layer of *Atrina* according to Weiner and Addadi. (Reprinted from [43] with permission.) The β-chitin lamellae are interspersed in a highly hydrated silk fibroin gel. The gel contains soluble *Asp*-rich glycoproteins, which can bind to the β-chitin surface by means of hydrophobic or electrostatic interactions. *Right*: Structure model of a putative nucleation site in molluscan tissues. The sulfate groups, linked to flexible oligosaccharide side chains, concentrate Ca^{2+} ions on an Asp-rich oligopeptide domain that is assumed to adapt a highly regular β-sheet conformation. A first layer of Ca^{2+} ions may thus be fixed and oriented in space upon which further mineral growth ensues. (Reprinted from [39] with permission)

interact with silk fibroin in the described way are oligopeptides containing sequence motifs of $[Asp\text{-}X]_n$, (X = Gly, Ser), which have a strong tendency to fold into a β-sheet conformation in the presence of Ca^{2+} ions [44]. As a consequence, the aspartic acid residues of $[Asp\text{-}X]_n$ sequences would be positioned at only one side of the β-pleated sheet, resulting in an organized 2-D array of carboxylate ligands.

It is tempting to assume that carboxylate residues coordinate a first layer of Ca^{2+} ions, which would in turn become the first layer of an epitaxially growing $CaCO_3$ crystal. However, studies have so far failed to provide evidence for an epitaxial growth mechanism or a close stereochemical complementarity between the nucleating macromolecules and the incipient $CaCO_3$ crystal surface. Rather, some properties of the mollusc shell ultrastructure point to less-sophisticated nucleation strategies: examination of the common crystal orientations in a variety of calcifying organisms reveals that aragonite and calcite single crystals most frequently nucleate from the *ab* planes. The arrangement of Ca^{2+} ions in this plane (the shortest distance between Ca^{2+} ions is 4.99 Å in calcite and 4.69 Å in aragonite, Fig. 2) is geometrically *not* commensurate with the period of amino acid residues in a protein β-strand (approx. 6.9 Å). Moreover – pointing more or less perpendicular to the Ca^{2+} ions in the *ab* plane – the carboxylate residues of the β-pleated sheet cannot continue the parallel arrangement of planar carbonate anions in the underlying layer(s). The current nucleation model thus does not support the picture of a calcite or aragonite single crystal being nucleated from (00.1) crystal faces by virtue of stereochemical selection principles and epitaxial crystal growth [45–47].

Despite the similar positioning of Ca^{2+} ions in the *ab* planes of calcite and aragonite, mollusc shells discriminate between the two polymorphs by secreting them separately in different layers (e.g., prismatic layer and nacre). This suggests that additional factors participate in nucleation. One possibility is that different Mg^{2+} concentrations in the fluids of aragonitic and calcitic layers may be present that could help to shift the balance between the two polymorphs. Another possibility is the presence of polymorph-specific macromolecules that interact with more than one face of the nascent crystal. For a valid explanation of selective nucleation of either polymorph, the current, essentially geometric model will have to be refined. Much is expected to be learned from the first 3-D structure of a "crystal nucleating" macromolecule, although its "active" conformation may depend on the accompanying insoluble organic matrix in the biological tissues. It is worth mentioning that there exists a (genealogically unrelated) group of crystallization-inhibiting proteins, the so-called antifreeze proteins (AFPs) [48, 49], for some of which precise X-ray structural data are now available. Some of these proteins assume rigid molecular conformations and prevent ice crystal nuclei from growing into larger crystals by specific adsorption to specific crystal faces. However, as Evans pointed out in a critical

review [50], the structural aspects of AFPs and proteins involved in biomineralization processes are quite different: in contrast to ice-interaction proteins, which typically adopt stable secondary structures (α-helix, β-sheet, β-helix, etc.), biomineral-interaction proteins typically adopt unfolded, open conformations, and, where mineral binding motifs have been identified, these sequences exhibit structural trends toward extended, random coil, or other unstable secondary structures.

It should also be noted that molluscs show a much wider variety of textures than indicated so far (other typological crystal textures include cross-lamellar or foliated shell structures) [51–53]. In many (but not all!) molluscs the outer shell is composed of calcite and the inner shell of aragonite displays a brick-like microstructure. Crystallographic texture analysis indicates that in the nacre of most molluscs, *c*-axes are oriented more or less perpendicular to the surface of the shell, but *a*-axis orientations display characteristic patterns. In some species (e.g., the shells of most land snails) the *a*-axes of the aragonitic platelets all have the same orientation, or they display a texture pattern with $\{110\}$ twinning as in *Nautilus*, or they spin randomly about the *c*-axis with a [001] fiber texture as in *Haliotis* (Abalone). Chateigner et al. surveyed a large number of mollusc species and concluded that the diverse texture patterns are related to phylogeny and presumably to the protein type [54].

From a materials scientist's point of view, nacre can be regarded as a *hierarchical* biological nanocomposite [56]. Though nacre is mainly composed of a brittle inorganic material, its highly organized design (Fig. 7) leads to extraordinary mechanical performance owing to an excellent combination of stiffness, strength, impact resistance, and toughness [57–59]. The structure of nacre has been reviewed repeatedly [60–62], and numerous reports indicate that nacre is composed of pseudo-hexagonal, polygonal, or rounded aragonite tablets having lateral dimensions of ~ 5–$20\,\mu$m and a thickness of ~ 0.3–$1.5\,\mu$m (as shown in Fig. 7). For gastropod nacre, SEM micrographs suggest that each aragonite tablet is subdivided by radial vertical organic membranes into a varying number of sectors (Fig. 7c), which have been interpreted to be polysynthetically twinned crystalline lamellae [63]; this interpretation, however, has been at least partly refuted by subsequent investigations [64].

The surface of nacre tablets (Fig. 7c) from California red abalone (*Haliotis rufescens*) possesses nanoasperities (~ 30–100 nm diameter and ~ 10 nm in height) [57, 65] and mineral "bridges" (Fig. 7b) (~ 25–34 nm in size, ~ 91–$116\,\mu m^{-2}$ surface density) between sheets that pass through the organic intertablet layers [19, 66]. The organic matrix constitutes the remaining ~ 5 wt % of the material. The intertabular polymer layer has a thickness varying between ~ 30 and 300 nm [67], with pores that allow the mineral bridges to pass through [66], and intracrystalline proteins present within the tablets themselves [21, 22].

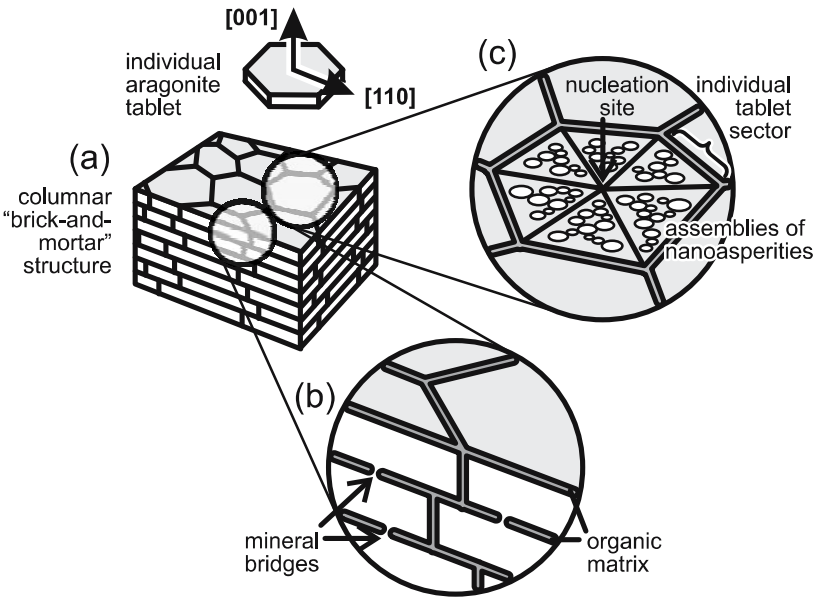

Fig. 7 Schematic illustration of the multiscale hierarchical structure of nacre: **a** 10 μm length scale, **b**, **c** 2 μm length scale, showing individual tablet features at a 200 nm length scale consisting of assemblies of nanoasperities. (Scheme redrawn after [55]). In "columnar" nacre, the tablets are relatively uniform in size and stacked vertically along the *c*-axis direction (with a slightly staggered arrangement laterally), thereby forming microlaminate sheets and tessellated bands. A domain structure has been found parallel to the *c*-axis direction consisting of 3–10 tablets with *a*-axes parallel to each other, while in the plane of the sheet, the *a*-axis orientation is variable

A natural adhesive protein (*Lustrin A*) has been isolated from the organic matrix of California red abalone nacre and was found to have a "modular" structure, i.e., a multidomain architecture composed of folded, nanometer-sized modules, covalently linked together in series along a single macromolecular chain [27]. While the primary structure of *Lustrin A* has approximately ten alternating Cys- and Pro-rich domains, it contains only a very short polyelectrolyte ("acidic") segment that could be responsible for attachment to the mineral surface [68]. It is not yet clear whether *Lustrin A* has a functional role similar to the acidic water-soluble proteins summarized in Table 3. However, a biophysical model of its elastic properties has been proposed that relates its modular structure to the mechanical toughness and fracture resistance of nacre [69].

This short summary of mollusc shell formation and the morphological properties of nacre indicates that the biological growth processes involved are much more complex than the seemingly primitive, brickwork-like structure might at first glance suggest. Nevertheless, scientists have sought out different kinds of bottom-up approaches to mimic different aspects of the molluscan mineralization system [70]. Especially, the quest for a possible epitaxial relation between the organic matrix and the overgrowing inorganic crystals has been subject of many experimental studies.

4
Crystallization of $CaCO_3$ Beneath Monolayers

4.1
Experimental Setup for the Growth of Inorganic Crystals Beneath Monolayers

Several studies have been devoted to the putative mechanisms underlying the formation of highly organized mineral structures in molluscs and similar organisms. Due to the various experimental difficulties of observing crystal growth in living molluscs, scientists have sought out suitable model systems for biomineralization processes reflecting the mineral/matrix interactions active at the atomic or molecular level of structural complexity. Seminal contributions were made by Mann and Heywood, who studied the influence of charged monolayers on crystal nucleation [71]. The group made use of a Langmuir film balance that allows for the spreading of surfactant molecules as a water-insoluble monolayer at the air–water interface. The basic principle of the experimental setup is shown in Fig. 8, in which the surfactant molecules are symbolized by a wire-model of hydrocarbon chains and the charged head groups (symbolized by triangles) point toward the aqueous subphase.

In studies relating to the biomimetic crystallization of $CaCO_3$, a freshly prepared ~ 9–10 mM aqueous solution of $Ca(HCO_3)_2$ is often used, which becomes instable with respect to the dissociation of bicarbonate anions into carbon dioxide and carbonate anions. Due to slow decomposition of the intermediate carbonic acid – yielding carbon dioxide and a water molecule – $CaCO_3$ precipitation is relatively slow (in the optical microscope, the first

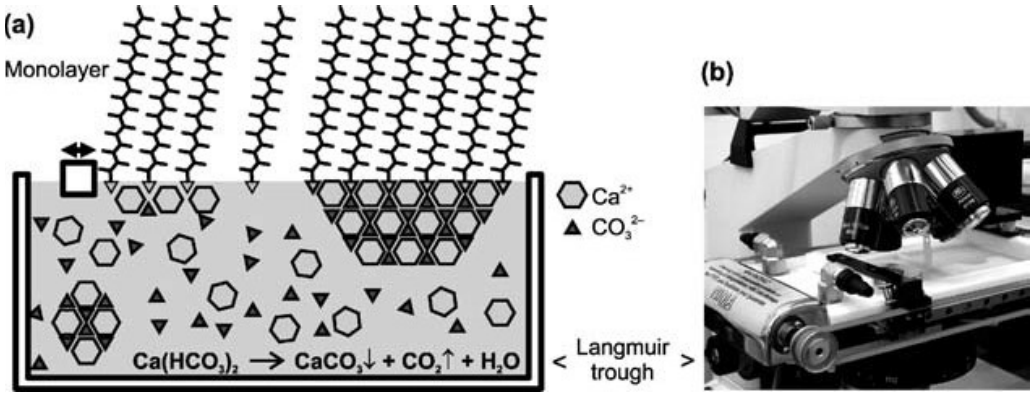

Fig. 8 **a** Illustration of a Langmuir film balance used for biomimetic crystallization of $CaCO_3$ and other inorganic phases beneath insoluble monolayers of amphiphilic molecules. **b** Computer-controlled miniature film balance replacing the stage of an optical microscope. The balance is equipped with two mechanically coupled barriers used for compression of the monolayer and a sapphire window, which permits the observation of crystal growth with transmitted light

macroscopic crystals become visible within some minutes to hours, depending on the experimental conditions). The slowness of crystal formation allows for adjustment of the compression state of the monolayer, i.e., to limit the average surface area available for a single molecule in the monolayer and/or to induce a monolayer phase transformation [72, 73].

The monolayer crystallization method has both technical advantages and disadvantages. As a general advantage, the use of a Langmuir film balance allows for creating a smooth and clean interface and for depositing a measured quantity of amphiphilic molecules in a controlled way. The average area per molecule is adjusted by a movable barrier, and the surface pressure or tension is monitored by a pressure sensor. The simple technical setup can be augmented by various analytical characterization methods, e.g., by Brewster-angle or fluorescence microscopy for imaging domain structures of the monolayer, or by surface potential measurements, to name just a few [72, 73]. In many cases it is straightforward to obtain a first-approximation model of the arrangement and packing of molecules in the monolayer. Over many years this technique has been used, mainly by the group of Leiserowitz and Lahav, to investigate epitaxy and chiral discrimination of molecular (non-ionic) crystals growing beneath specially designed monolayers [74, 75].

A technical disadvantage of the Langmuir setup is the mobility and the thinness of the monolayer, which renders structural investigations at high resolution (i.e., at the atomic or molecular level) a difficult task. In principle, it is possible to deposit a monolayer as a Langmuir–Blodgett film on a substrate surface and to employ surface analytical techniques, such as scanning force or tunneling microscopy, in order to obtain high resolution images of the interface structure. This strategy, however, has rarely been utilized in studies related to biomimetic crystallization [76].

A particular advantage of crystallizing calcium carbonate beneath monolayers is that the three main crystal polymorphs (i.e., calcite, aragonite, and vaterite) can be distinguished easily by their characteristic crystal habits. While aragonite and vaterite crystals normally adopt complex acicular or floret-type morphologies (see examples shown later in Fig. 20), calcite crystals often appear as sharply defined single crystals displaying the shape of a (truncated) $\{10.4\}$ cleavage rhombohedron (Fig. 9).

The orientations of calcite crystals with respect to the monolayer can be deduced from optical or scanning electron micrographs. A projection of rhombohedral faces onto the image plane yields characteristic interfacial angles, based upon which crystal orientations can be determined by comparing the measured angles and the general outline evident in micrograph images to computer-generated crystal models cleaved along various crystallographic planes (Fig. 9c). This procedure, however, strictly requires the sample to be aligned perpendicular to the viewing direction, while at the same time perspective aberrations of the optical system must be kept to a minimum. Owing to the fact that only a very limited number of crystal specimen can be

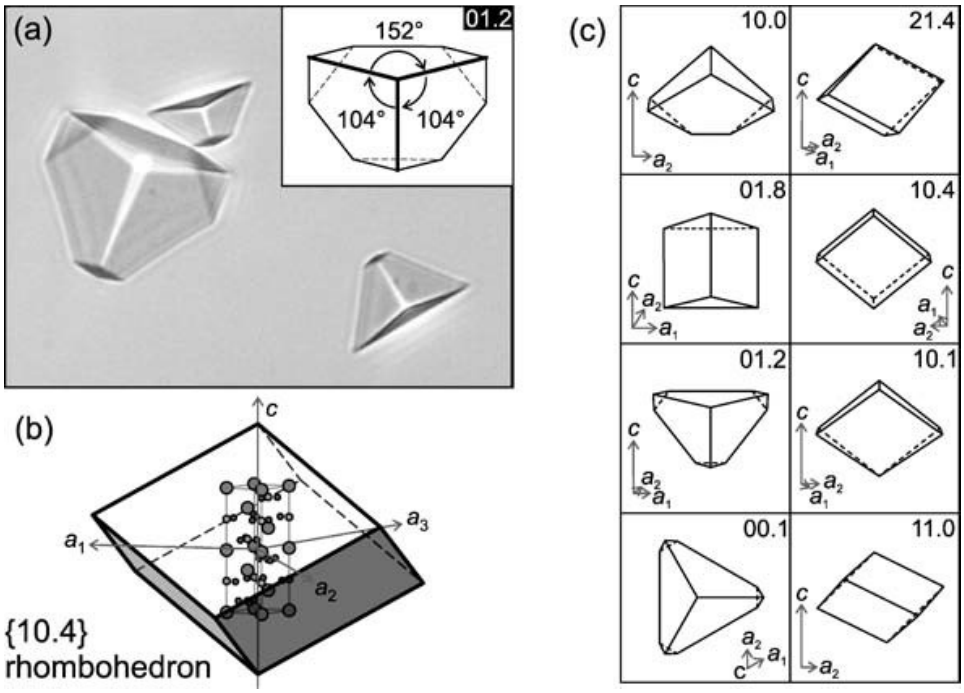

Fig. 9 **a** In situ optical micrograph of calcite crystals attaching to a monolayer. The *inset* shows the model of a truncated calcite {10.4} rhombohedron cut along its (01.2) plane. The displayed numbers represent interfacial angles of crystal edges projected onto the image plane. (Crystallographic angles between the edges of the {10.4} crystal face are 101.90° and 78.10°, respectively). **b** Model of a calcite crystal bounded by six symmetry-equivalent {10.4} faces. The *overlay* shows the orientation of the hexagonal unit cell of calcite with respect to the crystal edges. Lattice vectors a_i and c are sketched as *red arrows*. **c** Outlines of calcite single crystals cleaved along various crystallographic planes (specified by their Miller–Bravais indices). Models of crystals are oriented such that their cleavage planes coincide with the image plane

analyzed in this manner within a reasonable timeframe, the method suffers from the inherent disadvantage that crystals tend to be neglected when their orientations are difficult to determine (e.g., because the crystals are small) or when the crystals grow as polycrystalline aggregates. Unfortunately, there are no simple-to-use analytical techniques for simultaneously determining the phase composition, average crystallite size, and orientation distribution function (ODF) of the loose assembly of macroscopic crystals that is typically encountered in monolayer investigations. There *are* dedicated methods for these tasks, such as X-ray pole-figure measurements or automated analysis of Kikuchi line patterns using electron backscatter diffraction (EBSD) systems [77]. These methods, however, are not readily available for in situ measurements of crystal growth beneath monolayers, and they normally impose strict requirements on sample preparation, such as a uniform sample thickness or a flat (= polished) sample surface. Given the technical difficulties described above, any statements in the literature referring to the epitaxial growth of inorganic crystals beneath monolayers should be interpreted with

caution, since the presentation and evaluation of crystal orientation data are somewhat arbitrary. Moreover, many studies describing the heteroepitaxy of calcite crystals focus explicitly on the particular crystal texture of nacre, which, however, consists of aragonite and not calcite. The reason for the latter contradiction might lie in the fact that aragonite single crystals are difficult to prepare at ambient conditions [78–80], and they rarely manifest the pseudohexagonal shape of the tabular aragonite crystals that constitute the brick-and-mortar structure of nacre (Fig. 7).

4.2 Crystallization of $CaCO_3$ Beneath Monolayers of Simple Aliphatic Surfactants

Nucleation of calcite single crystals was observed with monolayers of aliphatic monocarboxylic acids, sulfates, or phosphonates as summarized in [81]. In general, the crystals that grew beneath monolayers showed a significantly narrower size distribution and reduced nucleation time in comparison to calcite crystals precipitated spontaneously from supersaturated solutions. Moreover, the crystals grew with preferential orientations relative to the monolayer. Calcite single crystals nucleated predominantly from the $\{10.0\}$ face underneath compressed monolayers of monofunctional amphiphilic carboxylic acids [82], while monolayers of alkylsulfates and -phosphonates led to calcite single crystals that nucleated from the $\{00.1\}$ face [83]. In contrast, monolayers of octadecylamine induced the precipitation of vaterite crystals, and monolayers of octadecanol inhibited crystal growth. Detailed schemes were proposed for rationalizing the different modes of interaction between the different head groups of amphiphiles in the monolayers and the corresponding faces from which the crystals were nucleated [84]. It was suggested that the orientation of calcite crystals growing below a monolayer is dictated by geometric and stereochemical complementarity between the (charged) headgroups of the monolayer and the ionic constituents of the nucleated crystal face. The outcome of these investigations was regarded as experimental justification for the "template model of biomineralization" discussed in the previous chapter. The seemingly clear and unequivocal interpretation of the crystal growth mechanism as an epitaxial phenomenon has stimulated a host of subsequent model investigations of the biologically inspired crystallization of inorganic solids beneath Langmuir monolayers. Many of the latter studies provided further impetus to the notion of the "molecular blueprinting" of inorganic materials by a pre-organized organic matrix.

Crystallization underneath monolayers of stearic acid (**1**) spread on aqueous calcium bicarbonate solution (9 mM), for instance, yielded two sets of morphologically distinct forms of calcite, termed type I and type II (Fig. 10) [82]. Both crystal morphologies nucleated from a (10.0) plane. The plate-like crystal habit at early growth stages changed into capped rhombohedral plates of type I crystals in mature crystals and a related triangular

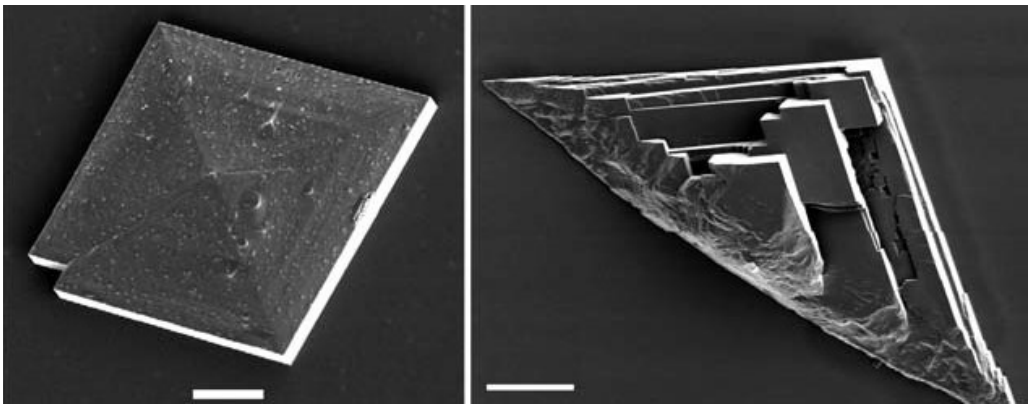

Fig. 10 Scanning electron micrographs of type I and type II calcite crystals nucleated from a {10.0} face beneath monolayers of **1**. *Scale bars* denote 10 μm. (Reprinted from [82] with permission)

morphology of type II crystals. When the Ca ion concentration of the subphase was reduced (4.5 mM), only vaterite crystals were observed, which is a quite remarkable result, since one would ordinarily expect the thermodynamically less stable crystal polymorph to form at *higher* supersaturation, rather than vice versa.

The preferential orientation of calcite crystals with respect to the monolayer plane was discussed in terms of a geometrical and stereochemical match between the stearic acid monolayer and the nucleated crystal face. It was argued that the spacing of the carboxylate headgroups in the monolayer matches the spacing of carbonate ions in the {10.0} face of calcite. Stereochemical complementarity was suggested to exist between rows of anions in the {10.0} face of calcite – where the C_{2v} axis of the carbonate moieties is perpendicular to the cleavage plane of the crystal – and the arrangement of carboxylate head groups in the monolayer (Fig. 11).

Uniformly oriented calcite crystals were also produced underneath monolayers of eicosyl sulfate (**2**) and eicosyl phosphonate (**3**), but in contrast to stearate monolayers, the calcite crystals exposed their {00.1} face to the monolayer and developed an equilateral triangular shape. In contrast to stearic acid, the headgroups of eicosyl sulfate and eicosyl phosphonate exhibit trigonal symmetry, which could mirror the planar arrangement of carbonate ions in the {00.1} face of calcite. It was proposed that in this case the stereochemical complementarity overrides the approximate geometrical match between the monolayer and the nucleated crystal plane (Fig. 12) [83].

The dynamic behavior of fatty acids with different hydrocarbon chain lengths was characterized by Brewster-angle microscopy (BAM) and correlated to changes in crystal growth behavior [85]. While palmitic acid ($C_{15}H_{31}COOH$, **4**) simultaneously induced the growth of aragonite, vaterite, and non-oriented calcite crystals, tricontanoic acid ($C_{29}H_{59}COOH$, **5**) almost

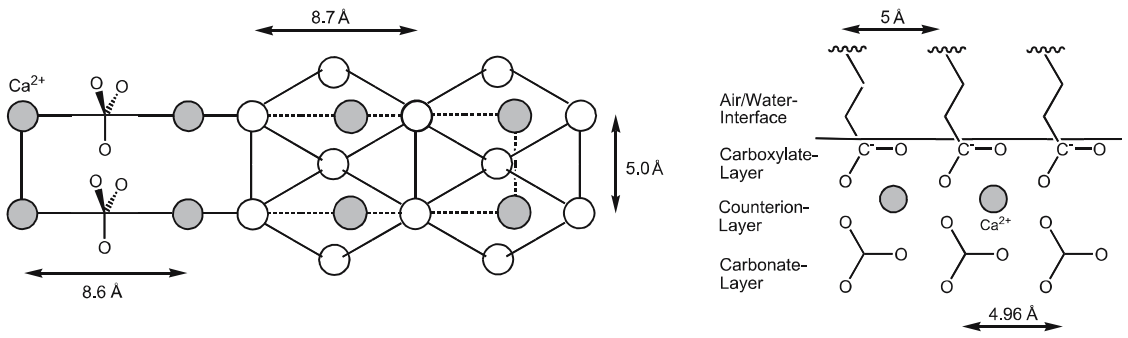

Fig. 11 **a** Schematic diagram showing the geometrical match between the headgroup spacing in the monolayer of stearic acid (**1**) and the carbonate–carbonate spacing in the {10.0} face of calcite. (*Gray dots* calcium ions, *white dots* carboxylate ions.) **b** Schematic diagram showing the stereochemical complementarity between the orientation of carboxylate groups of the monolayer molecules of **1** and the carbonate ions in the {10.0} face of calcite. (Redrawn after [82])

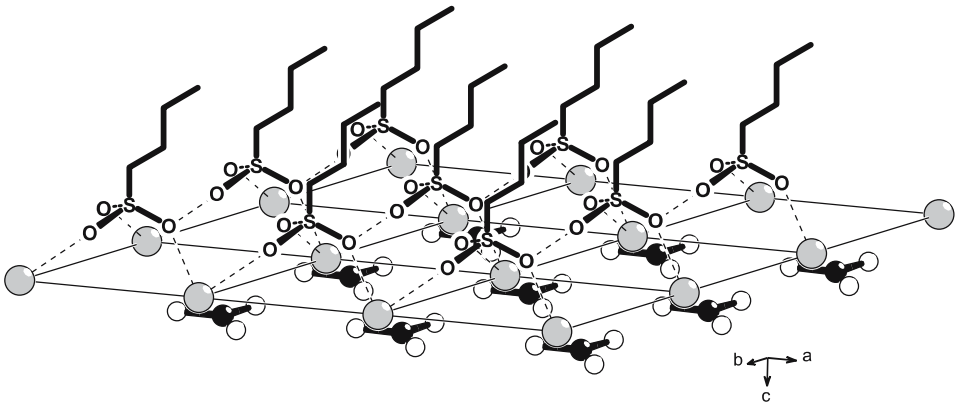

Fig. 12 Orientation of (00.1) oriented calcite crystal relative to monolayers of eicosyl sulfate or eicosyl phosphonate, according to Heywood and Mann [83]. Close-up of the interface between the monolayer of an anionic surfactant with a C_{3v}-symmetric headgroup (here: a sulfonate) and the (00.1) plane of the calcite crystal lattice. The selection of the (00.1) plane is dictated by a stereochemical and geometrical match between sulfonate groups and the underlying first layer of Ca ions. In the displayed μ_3-tridentate coordination mode, each sulfonate group replaces a CO_3^{2-} anion at a crystallographically equivalent position. Note, however, that the proposed isostructural replacement of CO_3^{2-} by $R-SO_3^-$ ions should lead to an unbalanced accumulation of charges, which constitutes an energetically unfavorable situation

exclusively led to the growth of uniformly (10.0) oriented calcite crystals having a triangular shape.

Polymorph selectivity was attributed to changes in the rate of carbon dioxide diffusion through the monolayer, indicating a kinetic effect. BAM analysis showed that the crystals preferentially nucleated under condensed monolayer domains and at domain boundaries, which was related to relaxation of the ordered monolayer structure. The size of condensed phase domains and the

amount of uniformly oriented calcite crystals grown beneath such domains increased with the chain length. Therefore, changes in crystal morphology were attributed to changes in the monolayer structure as a function of chain length.

Prior to these studies, monolayers of *N*-(10,12-pentacosadiynoyl)glycine (**6**) were analyzed by BAM [86]. Calcite crystals were found to grow beneath a monolayer of **6** at low surface pressure ($\pi = 0–5$ mN/m), where the BAM image of the monolayer indicated smectic domains. At high surface pressure ($\pi = 20$ mN/m), where the micrographs revealed a pseudo-focal-tonic monolayer texture, only vaterite was observed. It was pointed out that the distance between the foci of the monolayer texture almost exactly corresponds to the separation of the vaterite crystals, suggesting a spatial correlation between the monolayer and the crystals. In addition, it was argued that the monolayer packing density seems to play an important role in polymorph selection, since vaterite nucleation predominates at high surface pressure.

A well-defined alignment of $CaCO_3$ crystals was further achieved with polymeric Langmuir–Schaefer films of 10,12-pentacosadiyonic acid (**7**) [87].

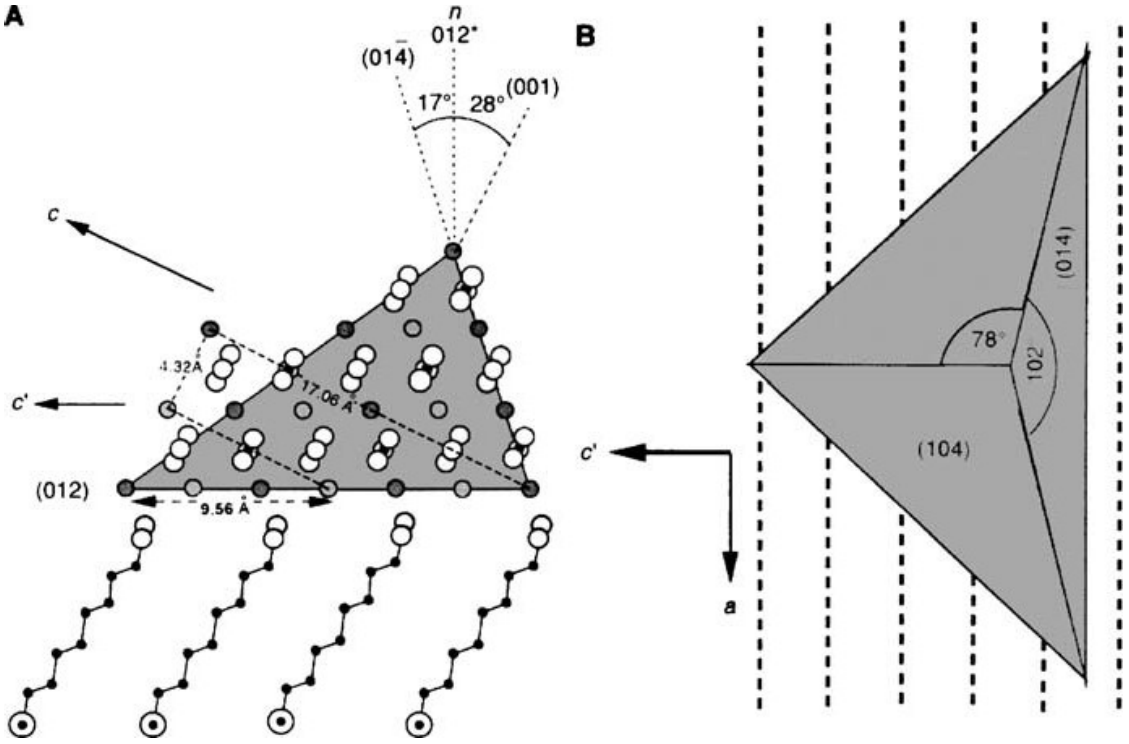

Fig. 13 Schematic diagram showing a potential geometric relationship between monolayers of **7** and the {01.2} face of calcite, according to [87]. *Left*: View along the *a* axis of calcite, down the polymer backbone direction and edge-on the (01.2) plane. Alternating calcium and tilted carbonate layers of the (01.2) plane of calcite are depicted. The calcite unit cell is shown as the *dashed, truncated rectangle*. *Right*: Schematic diagram of (01.2) oriented calcite single crystal with respect to the polymer backbone direction, indicating the dihedral angles

Langmuir monolayers of the monomeric 10,12 pentacosadiyonic acid first were polymerized with ultraviolet light and then transferred horizontally onto hydrophobized solid supports. Crystallization of $CaCO_3$ was performed by adding a drop of supersaturated $CaCO_3$ solution to the polymer film where the carboxylic headgroups were exposed to air. Calcite crystals nucleated from a {01.2} face and, moreover, in each single domain of the film of **7** they became co-aligned to each other with the crystals' *a*-axes oriented parallel to the polymer backbone. Along this direction both the (01.2) crystal plane and the polymer have a periodicity of about 5 Å, and a close geometric match between the carboxylate groups and the calcite crystal structure was proposed. To explain the nucleation of calcite from the {01.2} crystal face, a stereochemical complementarity between the monolayer and the crystal surface was suggested: in the {01.2} face of calcite, the carbonate ions are tilted 28° with respect to the normal of the (01.2) plane, a spatial arrangement that is matched by the 30° tilt of the side chains and carboxylate groups in the polymer (Fig. 13). The reorientation of side groups of the monolayer molecules upon crystallization was investigated by in situ FTIR measurements of the Langmuir–Schaefer films and interpreted as adaptability of the monolayer for achieving a stereochemical match [88].

4.3 Hydrogen Bonded Systems

Control over polymorph selection and calcium carbonate crystal orientations was also reported for self-organized hydrogen-bonded molecular ribbons consisting of monolayers of *N*,*N*′-dioctadecyltriazine-2,4,6-triamine mixed with different cyanuric acid derivatives as soluble component (**8**, Scheme 1) [89]. Residues of $-CH_2-CH_2-R$ were appended to the cyanuric acid moiety, differing in the functional groups R that point into the aqueous subphase. For monolayers comprised of alcohol (R = OH), amino (R

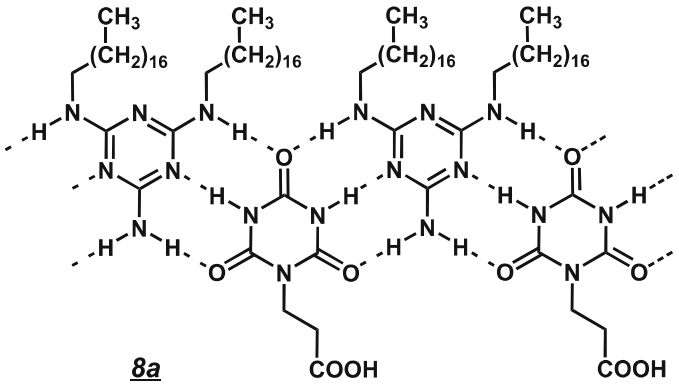

8a

Scheme 1 Structural formula of **8a**. Monolayers of *N*,*N*′-dioctadecyltriazine-2,4,6-triamine self-organize with a carboxylic acid derivative of cyanuric acid at the air–water interface

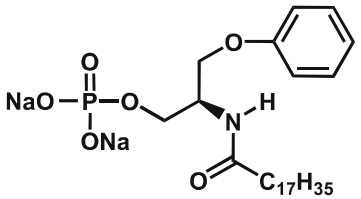

9

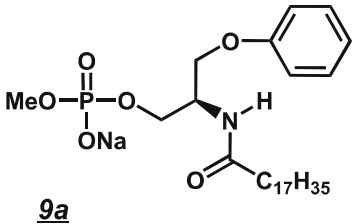

9a

Scheme 2 Structural formula of disodium (–)-(2S)-3-phenoxy-2-octadecanoylaminopropan-1-yl phosphate (**9**) and the corresponding methoxy derivative (**9a**)

= NH_2), or phosphate groups (R = OPO_3^{2-}), the observed crystal growth results resembled those of simple aliphatic surfactants possessing the same head group R. The carboxy-terminated derivative (**8a**, R = COOH) induced formation of (01.2) oriented calcite crystals. Again, control over crystal orientation was attributed to a geometrical and stereochemical matching between the putative positions of the functional groups R in the monolayer and the positions of ions in the adjacent calcite crystal face, although the periodicity and arrangement of functional groups in the monolayer of **8a** should differ significantly from the positions of the carboxylate residues in the Langmuir–Schaefer film (**7**) described above, which nevertheless led to the same (01.2) orientation of the crystal specimen.

By analogy to stearic acid (**1**), the nucleation and growth of (10.0) oriented calcite crystals has been reported for structurally different monolayers forming a network of strong intermolecular hydrogen bonds, such as (–)-(2S)-3-phenoxy-2-octadecanoylaminopropan-1-yl phosphate (**9**) or dioleyl phosphatidyl ethanolamine modified with (Leu – Glu) octapeptides (**10**) [90, 91]. Monolayers of **9** induced the crystallization of oriented calcite crystals either in a condensed liquid or in a solid monolayer phase, whereas monolayers of the methyl-substituted derivative (**9a**) having a decreased charge density yielded the same results in a solid monolayer phase only. The effect was related to geometrical lattice matching and stereochemical complementarity, as well as to the structural reorganization of molecules of **9a** arising from the state of compression. In addition to a proposed geometrical match between lipopeptide **10** and the {10.0} face of calcite, the observed epitaxy was attributed to the ability of the flexible monolayer to adapt to geometric constraints of the nucleated inorganic phase.

4.4
Aragonite Crystallization Induced by Monolayers of Bifunctional Surfactants

Monolayers of 5-hexadecyloxyisophthalic acid (**11**) induced the formation of acicular aragonite crystal aggregates at medium surface pressure (π = 10 mN/m) and at an ionic composition of the aqueous subphase that would normally yield the thermodynamically more stable calcite [92]. It was pos-

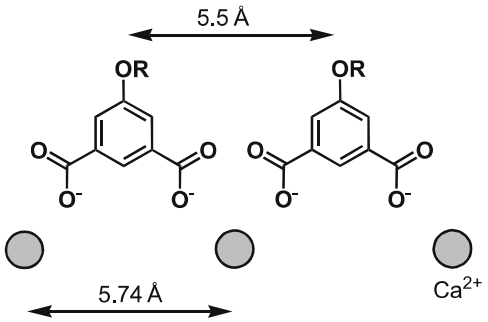

Fig. 14 Diagram showing the geometrical match between the headgroup spacing in the monolayer of **11** and the spacing of Ca^{2+} ions (*gray circles*) in the *c* direction of aragonite, according to [92]

tulated that the molecules (**11**) form a periodic arrangement on the aqueous subphase in such a way that the carboxylate groups are displaced by 4.4 Å in the *a* direction and 5.5 Å in the *c* direction, which corresponds geometrically to the position of Ca ions in the *ac* face of aragonite (Fig. 14). It was furthermore proposed that a bidentate coordination motif of the carboxylate substituents could complement the stereochemical arrangement of the carbonate groups in the *ac* face.

4.5 Crystallization of $CaCO_3$ beneath Monolayers of Macrocyclic Amphiphiles

The partially contradictory experimental findings reported for the growth of calcium carbonate beneath structurally different insoluble monolayers led us to design a small library of macrocyclic amphiphiles, which we based on calix[*n*]arene (*n* = 4,6,8) and resorc[4]arene moieties, respectively.

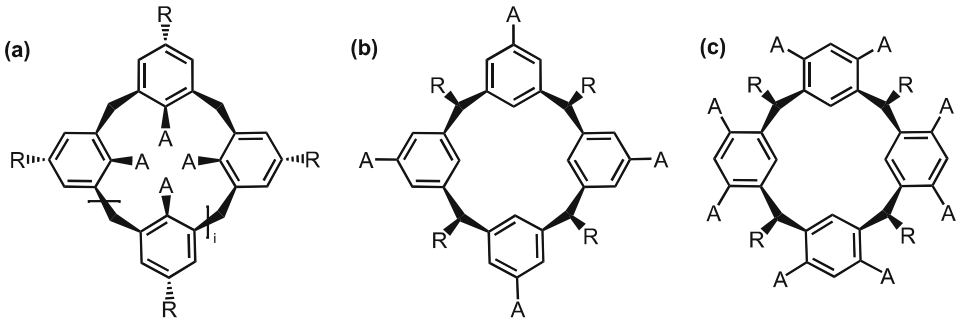

Scheme 3 Structural diagrams of calixarene (**a**, *i* = 0, 2, or 4), and resorcarene macrocycles (**b**, **c**) used in monolayer investigations, where R represents a strongly hydrophobic residue, and A represents an acidic (= metal ion coordinating) group. Although many different ring sizes and substitution patterns might be realized experimentally, few derivatives can be synthesized efficiently, due to their amphiphilic and multifunctional nature and the existence of different interchanging conformers

The use of these particular compounds might be rationalized in terms of their modular structure, which allowed us to synthesize amphiphilic compounds of different sizes and shapes, varying charge distributions and stereochemical arrangements of the coordinating head groups A (Scheme 3). In order to distinguish as much as possible between the various physical parameters that are known to influence the epitaxial growth of inorganic crystalline materials, we defined several working hypotheses that we tested in comparative crystal growth studies.

In a first set of experiments, the growth of calcite crystals beneath monolayers of the tetracarboxy-calix[4]arenes – namely, 5,11,17,23-tetrakis-(1,1,3,3-tetramethylbutyl)-25,26,27,28-tetra(carboxymethoxy)calix[4]arene (**12**) and 5,11,17,23-tetra-*t*-butyl-25,26,27,28-tetrakis(carboxymethoxy)calix

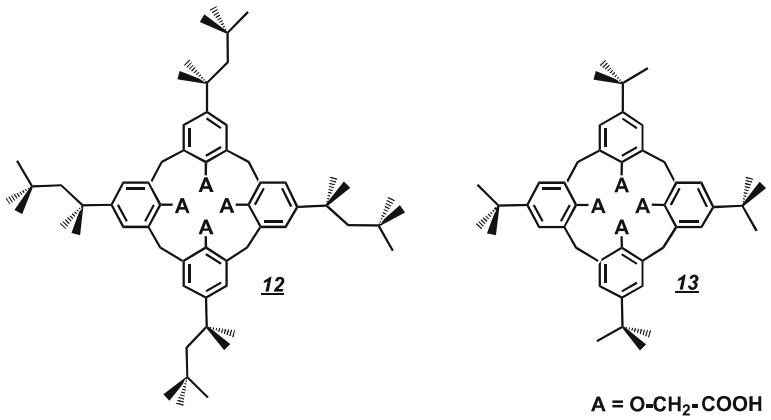

Scheme 4 Structural formulae of tetracarboxy-calix[4]arenes (**12**, **13**) bearing different hydrophobic substituents. The average area/molecule of **12** in a compressed monolayer is more than 15% larger than the corresponding value of **13** (at equal surface pressure)

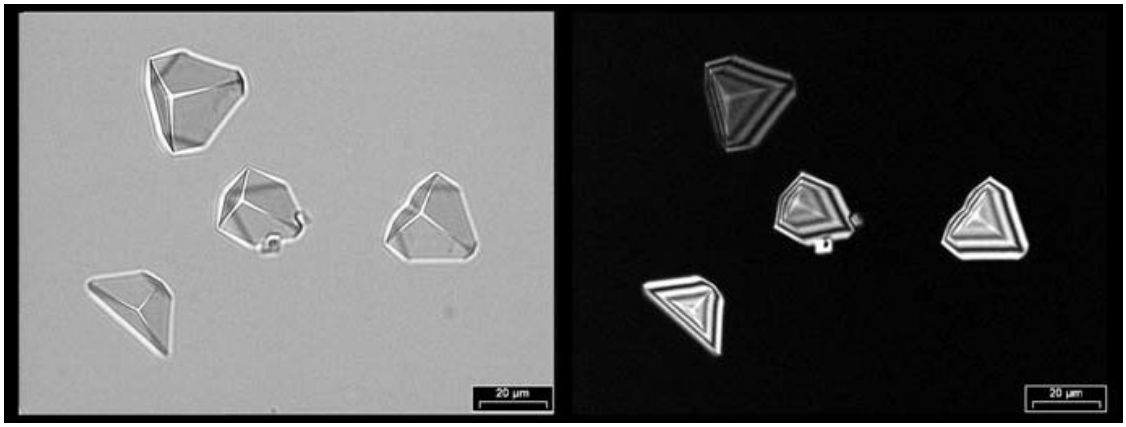

Fig. 15 *Left*: Optical micrograph (*bright field*) of (01.2) oriented calcite single crystals grown under a monolayer of **12** and **13**, respectively, after 3 h ($\pi = 0.1\ \mathrm{mN\,m^{-1}}$, $[Ca(HCO_3)_2]_{t=0} = 9$ mM). *Right*: Same crystal specimen observed in plane polarized light. The viewing direction is parallel to the monolayer surface normal, and crystals are observed from below the aqueous subphase. (Reprinted from [93] with permission)

[4]arene (**13**) – were investigated, which differ from each other by *the bulkiness of hydrophobic substituents* at the upper-rim of the macrocyclic backbone (Scheme 4).

Crystal growth experiments have shown that the same uniformly (01.2) oriented calcite single crystals grow beneath monolayers of **12** as well as **13** (Fig. 15) [93, 94]. The fact that identically oriented calcite crystals are obtained under monolayers of differently sized calix[4]arenes gives a strong indication *against* the assumption that an epitaxial match between the monolayer and the juxtaposed crystal surface is required for inducing a certain crystal growth behavior. However, according to these results it was still possible that the calix[4]arene ligands **12, 13** might afford a common, highly specific coordination motif by which they could bind to the {01.2} crystal face of the overgrown calcite crystals.

4.6 Influence of Coordination Geometry

In order to answer this critical question, a second type of macrocyclic ligands, the tetracarboxy-resorc[4]arene *rccc*-5,11,17,23-tetracarboxy-4,6,10,12,16,18,22,24-octa-*O*-methyl-2,8,14,20-tetra(*n*-undecyl)resorc[4]arene (**14**; Scheme 5), was designed and used in crystallization assays [95].

The single crystal X-ray structure analysis of a number of Ca^{2+} complexes of **12, 13** and **14** showed that the typical Ca^{2+} coordination motifs of these ligands are largely different (Fig. 16) [93–95]. However, in spite of these fundamental differences in molecular structure, crystallization assays employing monolayers of **14** gave (01.2) oriented calcite crystals that were virtually indistinguishable from those that grew beneath monolayers of **12** or **13**.

This unexpected experimental observation led us to examine the phase behavior of **12, 13** and **14** monolayers in more detail, for which we simultaneously recorded Langmuir and surface potential isotherms. Brewster-angle microscopy (BAM) images were taken for monolayers at different compression states.

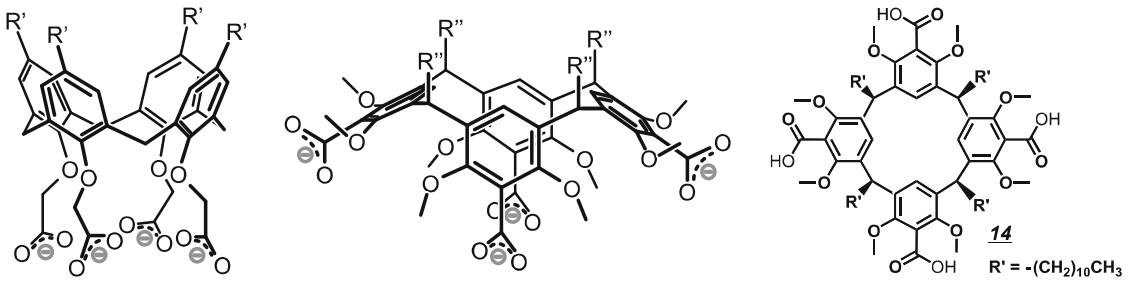

Scheme 5 *Left*: Typical arrangements of carboxylate moieties in calix[4]arene-type (**12, 13**) and resorc[4]arene-type (**14**) ligands (R′ *tert*-butyl or *tert*-octyl, R″ *n*-undecyl). *Right*: Structural formula of tetracarboxy-resorc[4]arene **14**, which according to X-ray analytical investigations and NMR studies assumes a C_{2v}-symmetric *boat* conformation [95]

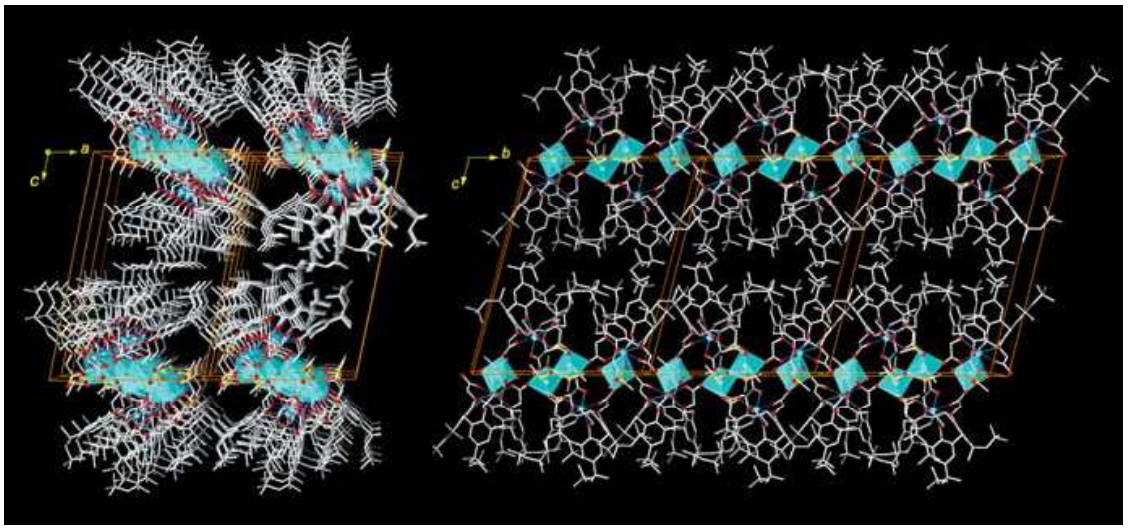

Fig. 16 Wire model of the coordination polymer of the calcium complex of **12** showing the packing arrangement of the one-dimensional polymeric strands in the crystal lattice. Solvent DMSO molecules occluded in the crystal lattice and hydrogen atoms are omitted for clarity. Coordination polyhedrons are displayed for interconnecting Ca ions only. (Reprinted from [93] with permission)

In summary, the results of these investigations demonstrated that neither calixarene nor resorcarene derivatives have a tendency to form highly ordered liquid-crystalline phases during compression. Moreover, the growth of (01.2) oriented calcite crystals exclusively occurred at low surface pressure ($\pi = 0.1-1\ \mathrm{mN\,m^{-1}}$), where the monolayers show a transition from the liquid-expanded to the liquid-condensed state of matter. The morphology of

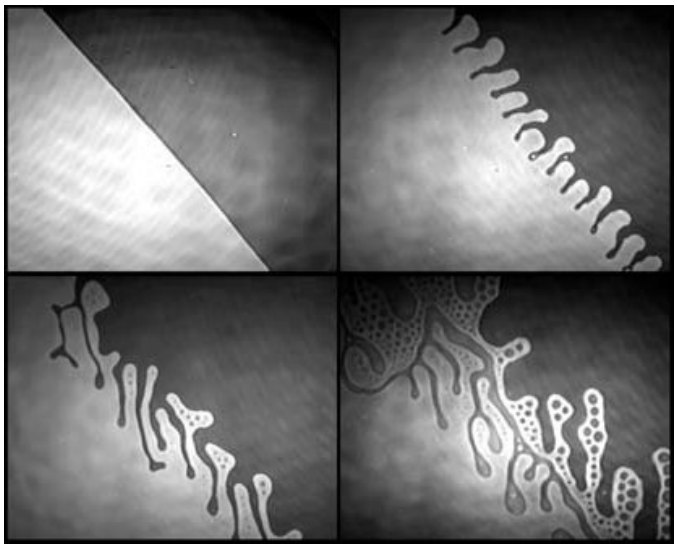

Fig. 17 Typical BAM micrographs of monolayers of **12** at 24 °C on 10 mM $CaCl_2$. Monolayer domains appear as *light regions*. All micrographs were recorded at identical surface pressure ($\pi = 0.1\ \mathrm{mN\,m^{-1}}$) within a period of 5 min. (Scanned image area $450 \times 400\ \mu\mathrm{m}$.) (Reprinted from [93] with permission)

the monolayer in this pressure regime is characterized by a high mobility of the molecules, as can be concluded from the typical foamy texture observed in BAM micrographs (Fig. 17).

4.7 Influence of Surface Charge Density

In order to gain additional insight into the interactions between monolayers and hydrated calcium and carbonate ions, the *non-charged* amphiphilic alcohol 5,11,17,23-tetrakis-(1,1,3,3-tetramethylbutyl)-25,26,27,28-tetra(2-hydroxyethoxy)calix[4]arene (**15**) was employed. Monolayers of **15** were found to strongly inhibit heterogeneous nucleation of $CaCO_3$ crystals [96]. The surface potential of a monolayer arises from the dipole moment of the constituent molecules, from the change of orientation of water molecules, and also from interactions between the headgroups and electrolytes dissolved in the subphase [97–99]. In this study electrostatic interactions between monolayers of structurally related amphiphilic calix[4]arene derivatives **12** and **15** and subphase ions was examined. In the low pressure region (π = 0.0–0.5 mN/m) of the monolayer phase diagram, the experimental surface potential values for monolayers of **12** and **15** on H_2O are almost identical. On a Ca-containing subphase (10 mM $CaCl_2$) the surface potential shows a significant increase only for monolayers of **12**, which clearly demonstrates that the calix[4]arene derivative **15** is unable to bind Ca ions by virtue of electrostatic and/or coordinative interactions. Furthermore, the experimental results indicated that a *low* surface pressure (π = 0.1–0.5 mN/m) is a necessary condition for the growth of uniformly (01.2) oriented calcite crystals. The phase diagram of **12** and previous investigations of the monolayer structure show no indication for long-range order in the monolayer – that is, the x and y-components of the molecular dipole moments are laterally uncorrelated.

The growth of calcite single crystals showing a preferential (01.2) orientation has been reported for other monolayer systems, including the polymeric Langmuir–Schaefer films of 10,12-pentacosadiynoic acid (**7**) mentioned above, as well as hydrogen-bonded molecular ribbons (**8**). Much effort has been spent in correlating the periodicity of the calcite {01.2} cleavage plane with the proposed monolayer structures (although experimental evidence, such as crystallographic investigations of characteristic molecular packing arrangements and Ca ion coordination motifs, has not been presented). However, it is hard to believe that the coincident growth of (01.2) oriented calcite crystals beneath structurally highly dissimilar monolayers is a consequence of a strict geometrical or even a stereochemical matching. In fact, this coincidence (that we laxly designate the "012-syndrome" in our group), indicated to us that non-directional interactions between the monolayer and the juxtaposed crystal face might be the most important factor.

To further support this hypothesis the crystallization of $CaCO_3$ below monolayers of two structurally different macrocyclic octacarboxylic acids, *rccc*-4,6,10,12,16,18,22,24-octakis-*O*-(carboxymethyl)-2,8,14,20-tetra(*n*-undecyl)resorc[4]arene (**16**) and 5,11,17,23,29,35,41,47-octakis-(1,1,3,3-tetramethylbutyl)-49,50,51,52,53,54,55,56-octa(carboxymethoxy)-calix[8]arene (**17**), were investigated (Scheme 6) [100]. Compounds **16** and **17** were chosen for these investigations because they differ by a factor of two in molecular surface area. It is thus possible to adjust the surface charge density underneath monolayers by a proper molecular design.

Interestingly, $CaCO_3$ crystallization beneath monolayers of **17** led to the formation of (01.2) oriented calcite crystals, despite the fact that the monolayer of **16** manifests a completely different growth characteristic: namely, the formation of acicular aragonite crystal aggregates at high surface pressure and at an ionic composition of the aqueous subphase that would normally yield the thermodynamically more stable calcite (Fig. 18).

In summary, these investigations provide compelling experimental evidence that the crystallization of $CaCO_3$ below monolayers of amphiphilic polyacids is largely controlled by the *surface charge density* that accumulates underneath the monolayer. Unfortunately, this functional correlation is difficult to confirm, since there exists (to the best of our knowledge) no analytical technique for measuring the absolute value of the surface charge density beneath the monolayer. The measurable *surface potential* of a monolayer is dependent on many factors, including the molecular structure of the surfactant, the packing arrangement and the composition of the aqueous subphase [97–99]. Moreover, it is not clear whether control over crystal nucleation by an increased surface charge density is gained through polarity matching between the surface monolayer and the incipient crystal surface, or if crystal nucleation and growth processes are kinetically controlled,

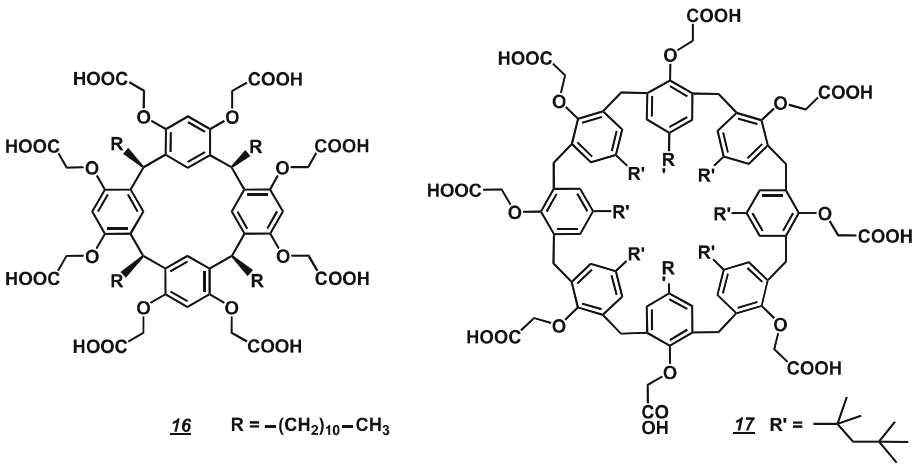

Scheme 6 Structural formulae of octacarboxy-resorc[4]arene (**16**) and octacarboxy-calix[8]arene (**17**) having the same number (= 8) of carboxylate residues but differing largely in molecular size

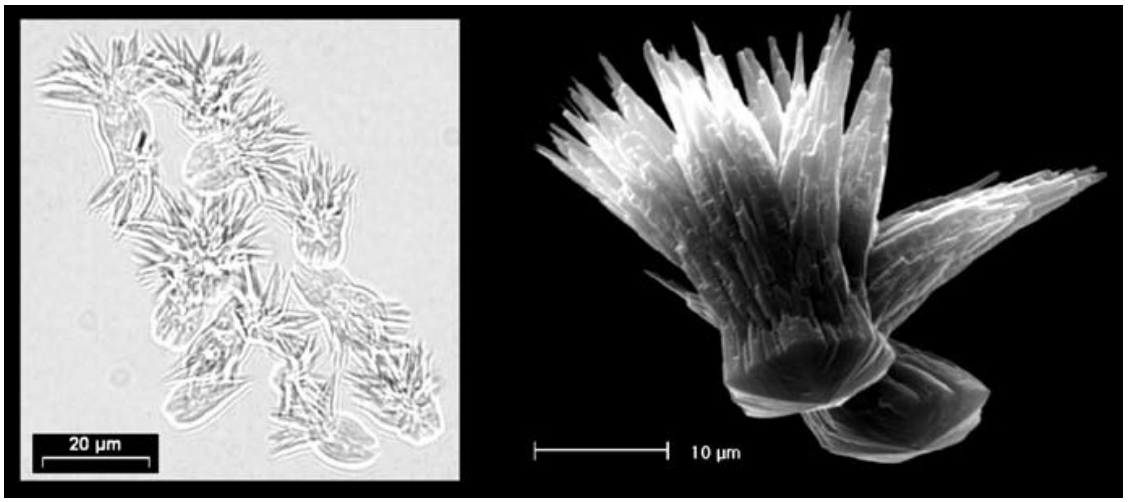

Fig. 18 *Left*: Bright-field optical micrograph of aragonite crystals grown beneath a monolayer of **16** after 3 h ($\pi = 20$ mN m^{-1}, $CaCl_2/NaHCO_3$ 9/18 mM)). *Right*: Scanning electron micrographs (crystals collected after 6 h) of crystals grown under a monolayer of **16**. (Reprinted from [100] with permission)

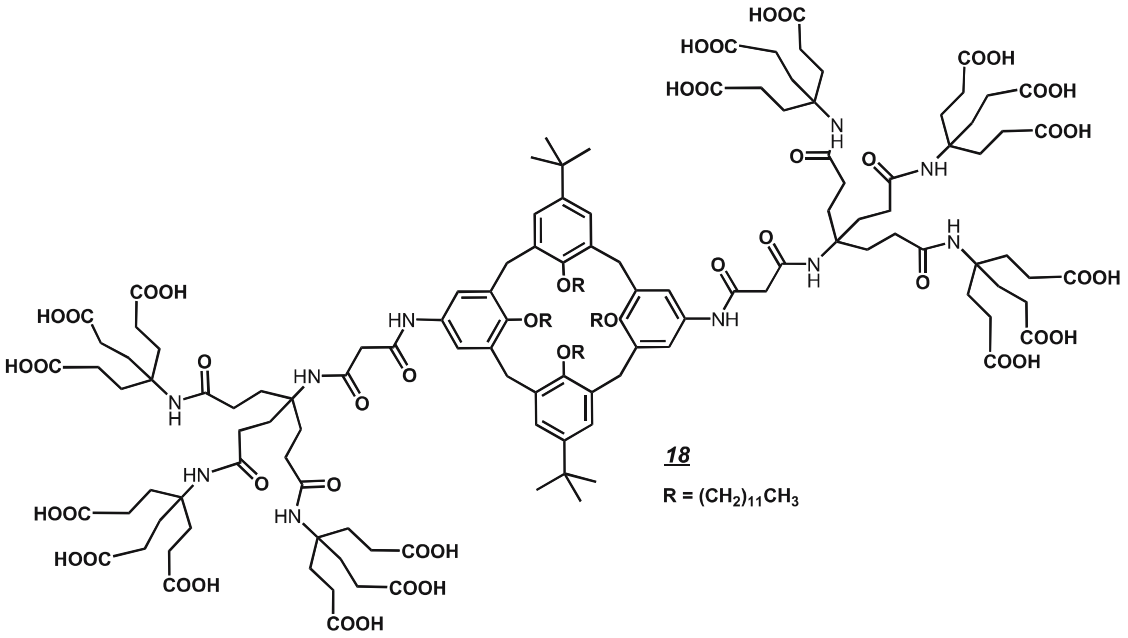

Scheme 7 Structural formula of the amphilic dendron-calix[4]arene (**18**) comprised of 18 carboxylic acid residues

or if both factors are equally important. In order to test whether monolayers generating a sufficiently high surface charge density are able to induce and stabilize metastable crystal phases at the air–water interface, the highly charged amphiphilic dendron-calix[4]arene, 5,17-di[(2-carboxyacetyl) amino]-11,23-di(*tert*-butyl)-25,26,27,28-tetradodecyloxycalix[4]arene [2]:(2-aza-3-oxopentylidyn):propanacid (**18**) was employed [101]. Indeed, crystallization of $CaCO_3$ beneath monolayers of **18** selectively led to growth of

the metastable polymorph vaterite at low surface pressure. Monolayers of **18** induce the formation of vaterite at a surface charge density corresponding to 6.7–7.2 COO^-/nm^2. On the other hand, surface charge densities in the range of 4.65–5.00 COO^-/nm^2 led to selective crystallization of aragonite, as was shown for monolayers of **16** and 5-hexadecyloxy-isophthalic acid (**11**), respectively. The formation of uniformly oriented calcite crystals with the highly polar {01.2} face oriented toward the monolayer was observed on many structurally different monolayers, all sharing similar charge densities of 2.0–2.4 COO^-/nm^2. A complete summary of the various carboxylic amphiphiles that have been used as crystallization templates and the $CaCO_3$ growth morphologies that they induce is given in Table 4.

Table 4 Correlation between area/molecule of amphiphiles used as crystallization templates and the $CaCO_3$ growth morphologies that they induce

Compound	Area/molecule		Area/molecule at which $CaCO_3$ crystals were grown [nm^2]	Charges in headgroup/nm^2	Polymorph (pref. orientation, if any)	Refs.
	Monolayer data [nm^2]	Crystal data [nm^2]				
1	0.23–0.24 [b]	n.d.	0.22–0.23	4.35–4.44	Calcite (10.0), vaterite	[82]
2	0.26 [b]	n.d.	n.p.		(00.1)	[83]
3	0.23 [b]	n.d.	n.p.		(00.1)	[83]
6	n.p.	n.d.	π = 0–5 mN m^{-1} π = 20–25 mN m^{-1}		Calcite vaterite	[86]
8	0.50 [a]	n.d.	0.43–0.50	2.00–2.33	Calcite (01.2)	[89]
9	0.50 [b]	n.d.	0.60	3.33	Calcite (10.0)	[90]
9a	0.45 [b]	n.d.	0.40	2.50	Calcite (10.0)	
10	2.50 [b]	n.d.		1.90–2.00	Calcite (01.2), Calcite (10.0)	[91]
11	n.p.	0.43	π = 10 mN m^{-1}	4.65	Aragonite, vaterite	[92]
12	1.70–1.75 [b]	1.70	1.75–1.80	2.22–2.29	Calcite (01.2)	[93]
13	1.30–1.40 [b]	1.70	1.70–1.80	2.35–2.42	Calcite (01.2)	[94]
14	1.70–1.75 [b]	1.83	2.00–2.10	1.90–2.00	Calcite (01.2)	[95]
16	1.65–1.70 [a]	1.71				[100]
	1.80–1.85 [b]	n.d.	1.60–1.70	4.71–5.00	Aragonite, vaterite	
17	2.75–2.80 [b]	n.d.	3.30–3.50 2.60–2.70	2.29–2.44 2.96–3.08	Calcite (01.2) Calcite, vaterite	[100]
18	1.95–2.05 [b]	n.d.	2.50–2.70	6.70–7.20	Vaterite	[101]

n.d. not determined, *n.p.* not published

[a] H_2O: doubly deionized water, resistance 18.2 MΩ · cm

[b] $CaCO_3$, 9 mM

5
Formation of Tabular Aragonite Crystals via a Non-Epitaxial Growth Mechanism

As the number of investigations targeting the molecular blueprinting beneath monolayers steadily increased, a notable change of the current template model of biomineralization took place, such that the vital role of *amorphous precursors* in biologically induced mineralization processes was emphasized [102, 103]. This change in paradigm was stimulated by the discovery of thin layers of amorphous calcium carbonate preceding the formation of crystalline materials in different organisms [104, 105]. These reports – together with the fact that, to date, no monolayer model system has been able to produce the specific crystal morphology of pseudohexagonal tabular aragonite crystals found in nacre – has led us to modify the experimental conditions in monolayer investigations.

Previous studies performed using arachidic acid (**19**) or amphiphilic tricarboxyphenylporphyrin iron (III) μ-oxo dimers (**20**) had already shown that

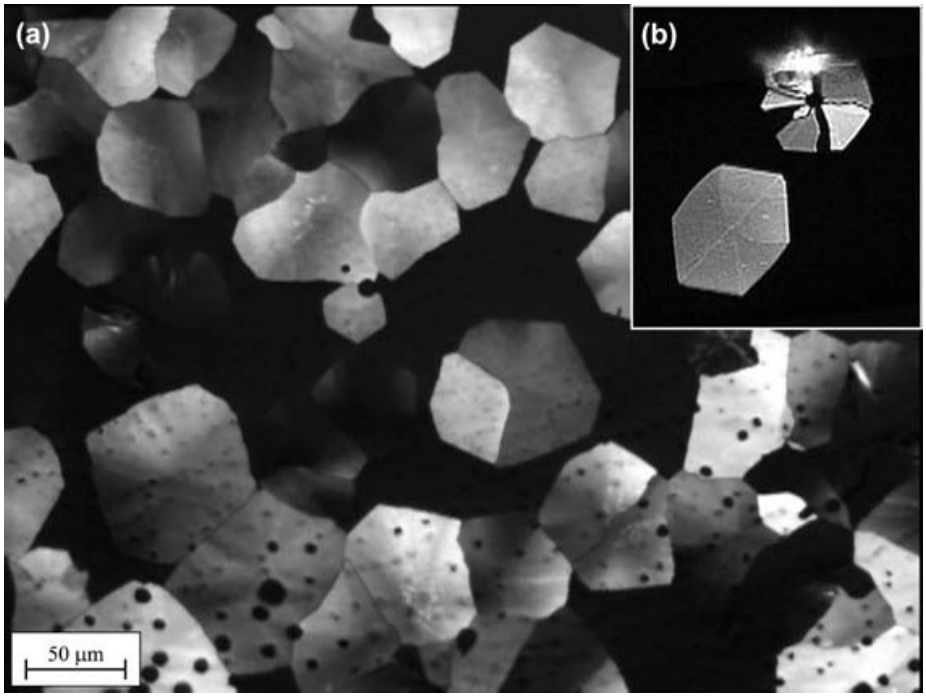

Fig. 19 **a** Polarization optical micrograph of polycrystalline calcium carbonate crystals grown from an amorphous thin film that forms beneath a monolayer of **14** when the aqueous subphase contains a growth inhibitor (polyacrylate). Holes inside the crystals are presumably due to the evolution of CO_2 bubbles from the aqueous subphase. **b** Close-up of two crystal specimens. The intact hexagonal platelet manifests sectors that might result from interpenetration twinning. The upper crystal has disintegrated into triangular sectors, the breakage presumably originating in the twinned contact planes of the crystal. Note that the pseudohexagonal shape and the twinning pattern are quite similar to those of the aragonitic platelets in biogenic nacre (Amos et al, submitted for publication)

a thin film of amorphous calcium carbonate might form below the monolayer if the subphase contains a soluble polyelectrolyte that acts as (non-specific) crystal growth inhibitor [106]. In the presence of polyacrylic acid, the fatty acid per calcium ratio is about 14–25, according to grazing-incidence X-ray diffraction measurements, and tablet morphologies of $CaCO_3$ most often resulted in the formation of calcite films [107].

Recently, the formation of single-crystalline aragonite (as well as calcite) tablets and films was accomplished by precipitating an amorphous precursor under conditions exploiting the synergistic effects of a monolayer of tetracarboxy-resorc[4]arene (**14**) and water-soluble additives, such as polyacrylic acid and/or magnesium ions (Amos et al, submitted for publication). Using appropriate concentrations of the latter, an initially amorphous film can be deposited beneath the monolayer that later crystallizes into polycrystalline films with either single-crystalline mosaic or spherulitic structure (Fig. 19a). Of particular importance is the synthesis of single-crystalline mosaic films of aragonite, which resemble the tablets of aragonite crystals in the nacreous layer of mollusc shells (Fig. 19b).

6 Conclusions

In the literature, the growth of inorganic materials below negatively charged monolayers is frequently considered to be a suitable model system for biomineralization processes. The fact that some monolayers give rise to oriented overgrowth of calcium carbonate crystals has been interpreted in terms of a geometrical and stereochemical complementarity between the arrangement of headgroups in the monolayer and the position of Ca ions in the crystal plane that attaches to the monolayer. The concept of the "molecular blueprinting" of ionic solids has partly arisen from the numerous astonishingly perfect crystal architectures found in biomineralizing organisms, the most prominent example of which is certainly provided by the "brick-and-mortar" structure of nacre. Until recently, the most widely accepted model for the emergence of nacre has suggested an epitaxy mechanism, according to which a highly ordered composite of crystal-nucleating acidic proteins and structural framework macromolecules (mostly chitin) acts as a supramolecular template matrix governing the site-selective and orientation-selective nucleation of the inorganic crystals. However, recent investigations of the structure of nacre provide strong evidence against this simple template hypothesis [108]. It turns out that the biosynthesis of an amorphous calcium carbonate precursor precedes formation of aragonite crystals. The mechanisms by which the amorphous phase is switched into a specific calcium carbonate polymorph and into crystals of particular shape are still largely unknown. However, by adapting model systems to this new paradigm, spe-

cific aspects of the complex biological growth processes might be suitably addressed.

Comparative investigations of the growth of calcium carbonate beneath monolayers of macrocyclic polyacids, for instance, have demonstrated that non-directional electrostatic parameters, such as the average charge density or the mean dipole moment of the monolayer, determine the orientation and the polymorph of the overgrowing crystals. A summary of the monolayer systems we have employed so far and the crystal morphologies they induce is given in Fig. 20.

Our results show that it is possible to control the surface charge densities in monolayers by the appropriate design of amphiphilic molecules. A polymorph switch occurs above a critical monolayer charge density at which aragonite or vaterite nucleation ensues, presumably due to a kinetically controlled precipitation process (Fig. 21a). Below this critical charge density value (for which, based on numerous monolayer investigations (Table 4), we may tentatively assign a value range of 3.5–4.5 COO^{-}/nm^{2}), calcite single crystals form. The sharply defined rhombohedral shape of these crystals and the fact that they show an island-like distribution beneath the monolayer provide a strong indication against epitaxial lattice correlations between the monolayer matrix and the incipient crystal face. Moreover, monolayers consisting of structurally

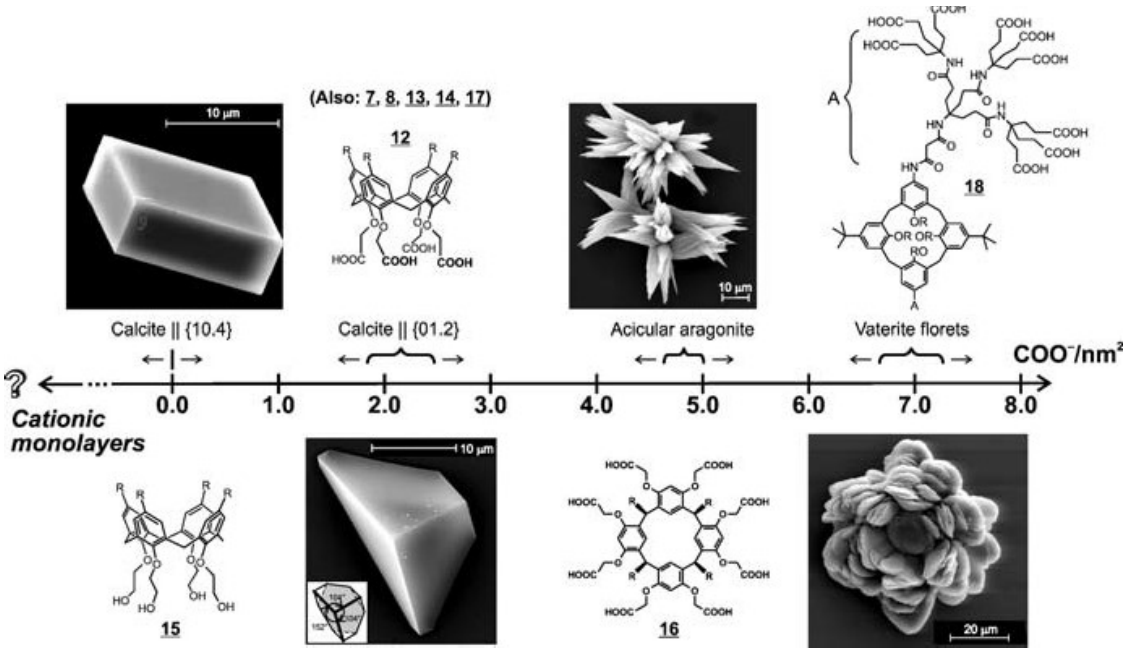

Fig. 20 Overview of macrocyclic polyacids employed in previous investigations of the growth of calcium carbonate beneath monolayers. Polyacids are arranged according to increasing (negative) charge density, which is expressed here as the number of carboxylate residues per unit area. Experimental ranges of charge density leading to a characteristic calcium carbonate crystal habit or orientation are indicated with *braces*. (Charge density values are directly gained from Langmuir isotherms)

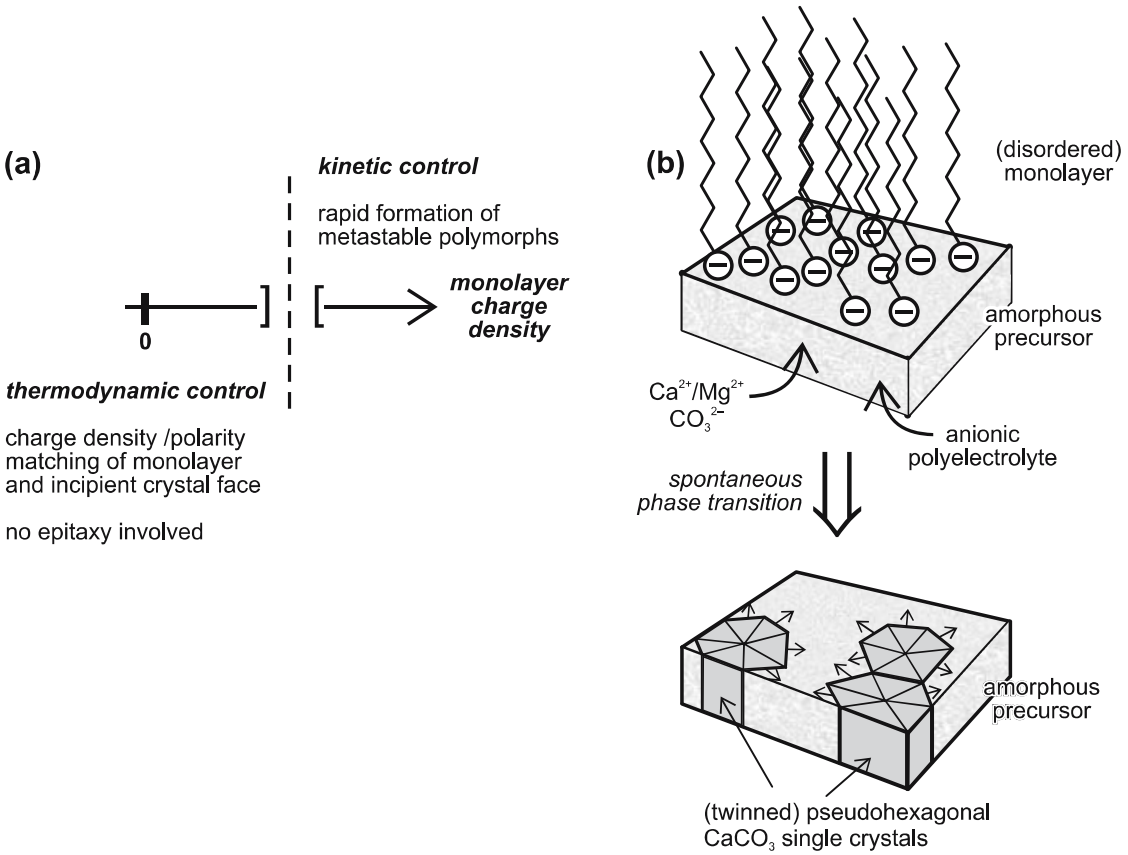

Fig. 21 **a** Scheme of charge density controlling the inorganic crystal polymorph that forms beneath the monolayer. For calcium carbonate, a switch from thermodynamically stable calcite to less-stable aragonite or vaterite occurs at a charge density ranging from 3.5–4.5 COO^-/nm^2. **b** Formation of polycrystalline thin films comprised of tabular pseudohexagonal calcium carbonate crystals via transformation of an amorphous precursor thin film. Recent investigations indicate that a similar phase transition occurs during the biological formation of nacre

very dissimilar amphiphiles often lead to identical crystal orientations, for which nucleation from the {01.2} crystal face of calcite is most often observed. We suggest that crystal nucleation occurs preferentially from this particular face because of charge density/polarity matching at the interface, considering that the {01.2} face is the most strongly polar (low-index) crystal face of the calcite crystal lattice. This hypothesis is further supported by recent modeling studies, which question the idea of stereochemical or geometrical complementarity between the monolayer and the nucleated crystal face [109, 110].

There are notable exceptions, such as monolayers of simple monofunctional surfactants, which lead to exceptional crystal growth orientations (e.g., alkyl sulfates leading to nucleation from the {00.1} crystal face or alkyl carboxylates nucleating calcite from a {11.0} face (Table 4)). However, more in-depth studies employing these simple surfactants once again have chal-

lenged the simple picture of interfacial complementarity. To give an example, the crystallization of $CaCO_3$ beneath fatty acid monolayers was studied by in-situ grazing incidence X-ray diffraction [111]. It was found that in monolayer systems of stearic acid (**1**) or arachidic acid (**19**), spread on 4.5 or 9 mM calcium carbonate solutions, there are only some four to eight surfactant molecules per calcium ion. A strict epitaxial correlation between the monolayer and the nucleated crystal would require a 1 : 1 or 2 : 1 ratio. This result demonstrates that the structure of the monolayer/crystal interface is very likely not as simple as suggested in preceding reports. Thus, it is safe to predict that there will be many more investigations in the near future targeting the fundamental mechanisms of crystal nucleation and growth beneath structurally mobile monolayers (without having to emphasize any model character that such systems may have for biomineralization processes!).

On the other hand, one of the most annoying and puzzling aspects of monolayer studies claimed as biomimetic model systems has been the fact that until very recently none of the systems has produced crystal morphologies reminiscent of aragonitic nacre, although this was implicit in the motivation of numerous studies. As we have stressed in this review, the main reason for this discrepancy is most likely an imperfect working hypothesis regarding the biological process of nacre formation itself. In fact, in recent model systems explicitly taking into account the multistepped formation process of biogenic nacre, including a phase transition from an amorphous precursor to a solid phase, many characteristic features of nacre could be reproduced in quite simple model systems [112].

Again, model systems employing monolayers as crystal growth matrices may provide novel insights into such transformations, as we have shown very recently when the aqueous phase contains a soluble polyelectrolyte (polyacrylate) and the Ca to Mg ion concentration ratio is adjusted appropriately. This system produces tabular pseudohexagonal calcium carbonate platelets, which occasionally show the characteristic crystal twinning pattern that is frequently reported for aragonite crystal platelets stemming from bivalve nacre. A shortcoming of the strategy for producing highly regular polycrystalline thin films according to Fig. 21b is the fact that the crystal texture of the film manifests significant variation from experiment to experiment (at least in our laboratory). Thus, the process requires further improvement if it is ever to be translated into a technically reliable production scheme for artificial nacre. A major leap towards this goal is certainly the development of processing strategies that lead to the deposition of *multilayered* crystal architectures. Recent progress in understanding natural biomineralization processes as well as experimental advances gained from model studies give rise to the hope that novel composite materials reminiscent of their biological counterparts might be produced at an industrial scale in the near future. It is very likely that some of these bionic materials will be constructed from totally different materials, since there is no urgent need to stick to calcium carbonate, chitin, or pep-

tides once the basic principles of biomineralization are clearly understood. The competition for attractive products has just begun [113].

Acknowledgements The authors are thankful to C.E. Krill III for proofreading the manuscript and providing critical comments. Financial support provided by the Deutsche Forschungsgemeinschaft (DFG Priority Program 1117, "Principles of Biomineralization", DFG grant Vo829/3) is gratefully acknowledged.

References

1. Weiner S, Addadi L (1997) J Mater Chem 7:689
2. Geisen M, Billard C, Broerse ATC, Cros L, Probert I, Young JR (2002) Eur J Phycol 37:531
3. Towe KM, Harper CW Jr (1966) Science 154:153
4. Gotliv BA, Addadi L, Weiner S (2003) ChemBioChem 4:522
5. Arias JL, Neira-Carrillo A, Arias JI, Escobar C, Bodero M, David M, Fernandez MS (2004) J Mater Chem 14:2154
6. Effenberger H, Mereiter K, Zemann J (1981) Z Kristallogr 156:233. ICSD no. 100676
7. de Villiers JPR (1971) Am Mineral 56:758. ICSD no. 15194
8. Meyer H-J (1969) Z Kristallogr 128:183. ICSD no. 18127
9. Effenberger H (1981) Monatsh Chem 112:899. ICSD no. 100846
10. Hesse KF, Kueppers H, Suess E (1983) Z Kristallogr 163:227. ICSD no. 31305
11. Morse JW, Mackenzie FD (1990) Geochemistry of sedimentary carbonate. Elsevier, Amsterdam, p 41
12. Lippmann F (1973) Sedimentary carbonate minerals, minerals, rocks and inorganic materials, vol 6. Springer, Berlin Heidelberg New York
13. Givargizov EI (1991) In: Oriented crystallization on amorphous substrates. Plenum, New York, p 10
14. Ward MD (2001) Chem Rev 101:1697
15. Carbone A, Prusinkiewicz P, Gromov M (eds) (2000) Pattern formation in biology, vision and dynamics. World Scientific, Hackensack NJ
16. Ball P (1991) The self-made tapestry: pattern formation in nature. Oxford University Press, USA
17. Simkiss K, Wilbur KM (1989) In: Biomineralization. Cell biology and mineral deposition. Academic, San Diego, p 230
18. Volkmer D (2000) In: Cooke M, Poole CF (eds) Encyclopedia of separation science, vol 2 (Crystallization). Academic, New York, p 940
19. Schäffer TE, Ionescu-Zanetti C, Proksch R, Fritz M, Walters DA, Almqvist N, Zaremba CM, Belcher AM, Smith BL, Stucky GD, Morse DE, Hansma PK (1997) Chem Mater 9:1731
20. Marin F, Luquet G (2004) C R Palevol 3:469
21. Belcher AM, Wu XH, Christensen RJ, Hansma PK, Stucky GD, Morse DE (1996) Nature 381:56
22. Falini G, Albeck S, Weiner S, Addadi L (1996) Science 271:67
23. Samata T, Hayashi N, Kono M, Hasegawa K, Horita C, Akera S (1999) FEBS Lett 462:225
24. Sudo S, Fujikawa T, Nagakura T, Ohkubo T, Sakaguchi K, Tanaka M, Nakashima K, Takahashi T (1997) Nature 387:563

25. Zhang Y, Xie LP, Meng QX, Jiang TM, Pu RL, Chen L, Zhang RQ (2003) Comp Biochem Phys B 135:565
26. Kono M, Hayashi N, Samata T (2000) Biochem Biophys Res Comm 269:213
27. Schen X, Belcher AM, Hansma PK, Stucky GD, Morse DE (1997) J Biol Chem 272:32472
28. Suzuki M, Murayama E, Inoue H, Ozaki N, Tohse H, Kogure T, Nagasawa H (2004) Biochem J 382:205
29. Sarashina I, Endo K (1998) Am Mineral 83:1510
30. Miyamoto H, Miyashita T, Okushima M, Nakano S, Morita T, Matsushiro A (1996) Proc Natl Acad Sci USA 93:9657
31. Marin F, Corstjens P, de Gaulejac B, de Vrind-De Jong E, Westbroek P (2000) J Biol Chem 275:20667
32. Mann K, Weiss IM, André S, Gabius H-J, Fritz M (2000) Eur J Biochem 267:5257
33. Weiss IM, Göhring W, Fritz M, Mann K (2001) Biochem Biophys Res Commun 285:244
34. Tsukamoto D, Sarashina I, Endo K (2004) Biochem Biophys Res Commun 320:1175
35. Michenfelder M, Fu G, Lawrence C, Weaver JC, Wustman BA, Taranto L, Evans JS, Morse DE (2003) Biopolymers 70:522
36. Fu G, Valiyaveettil S, Wopenka B, Morse DE (2005) Biomacromolecules 6:1289
37. Marin F, Amons R, Guichard N, Stigter M, Hecker A, Luquet G, Layrolle P, Alcaraz G, Riondet C, Westbroek P (2005) J Biol Chem 280:33895
38. Gotliv B-A, Kessler N, Sumerel JL, Morse DE, Tuross N, Addadi L, Weiner S (2005) ChemBioChem 6:304
39. Addadi L, Weiner S (1989) In: Mann S, Webb J, Williams RJP (eds) Biomineralization. VCH, Weinheim, p 133
40. Addadi L, Moradian J, Shay E, Maroudas NG, Weiner S (1987) P Natl Acad Sci USA 84:2732
41. Levi Y, Albeck S, Brack A, Weiner S, Addadi L (1998) Chem Eur J 4:389
42. Weiss IM, Renner C, Strigl MG, Fritz M (2002) Chem Mater 14:3252
43. Levi-Kalisman Y, Falini G, Addadi L, Weiner S (2001) J Struct Biol 135:8
44. Bertrand M, Brack A (1997) Origin Life Evol B 27:589
45. Weiner S, Traub W (1980) FEBS Lett 111:311
46. Weiner S, Traub W, Parker SB (1984) Proc R Soc B 304:425
47. Giles R, Manne S, Mann S, Morse DE, Stucky GD, Hansma PK (1995) Biol Bull 188:8
48. Yeh Y, Feeney RE (1996) Chem Rev 96:601
49. Davies PL, Sykes BD (1997) Curr Opin Struct Biol 7:828
50. Evans JS (2003) Curr Opin Coll Int Sci 8:48
51. Mayer G (2005) Science 310:1144
52. Wilmot NV, Barber DJ, Taylor JD, Graham AL (1992) Proc R Soc B 337:21
53. Taylor JD, Kennedy WJ, Hall A (1969) Bull Br Mus (Nat Hist) Zool Suppl 3:1
54. Chateigner D, Hedegaard C, Wenk H-R (2000) J Struct Geol 22:1723
55. Bruet BJF, Qi HJ, Boyce MC, Panas R, Tai K, Frick L, Ortiz C (2005) J Mater Res 20:2400
56. Jackson AP, Vincent JFV, Turner RM (1988) Proc R Soc London B Biol Sci 234:415
57. Wang RZ, Suo Z, Evans AG, Yao N, Aksay IA (2001) J Mater Res 16:2485
58. Jackson AP, Vincent JFV, Turner RM (1990) J Mater Sci 25:3173
59. Currey JD (1977) Proc R Soc London B Biol Sci 196:443
60. Erben HK (1974) Biomineralisation 7:14
61. Addadi L, Joester D, Nudelman F, Weiner S (2006) Chem Eur J 12:980
62. Lin A, Meyers MA (2005) Mater Sci Eng A 390:27

63. Mutvei H (1978) Zool Scr 7:287
64. Hedegaard C, Wenk H-R (1998) J Moll Stud 64:133
65. Li X, Chang W-C, Chao YJ, Wang R, Chang M (2004) Nano Lett 4:613
66. Manne S, Zaremba CM, Giles R, Huggins L, Walters DA, Belcher AM, Morse DE, Stucky GD, Didymus JM, Mann S, Hansma PK (1994) Proc R Soc London B 256:17
67. Watabe N (1965) J Ultrastruct Res 12:351
68. Wustman BA, Morse DE, Evans JS (2002) Langmuir 18:9901
69. Smith BL, Schäffer TE, Viani M, Thompson JB, Frederick NA, Kindt J, Belcher A, Stucky GD, Morse DE, Hansma PK (1999) Nature 399:761
70. Meldrum FC (2003) Int Mater Rev 48:187
71. Mann S, Heywood BR, Rajam S, Birchall JD (1998) Nature 334:692
72. Kaganer VM, Möhwald H, Dutta P (1999) Rev Mod Phys 71:779
73. Dynarowicz-Latka P, Dhanabalan A, Oliveira ON Jr (2001) Adv Colloid Interface Sci 91:221
74. Landau EM, Levanon M, Leiserowitz L, Lahav M, Sagiv J (1985) Nature 318:353
75. Weissbuch I, Lahav M, Leiserowitz L (2003) Cryst Growth Des 3:125
76. Zhang Y, Jin R, Zhang L, Liu M (2004) New J Chem 28:614
77. Wenk H-R, Van Houtte P (2004) Rep Prog Phys 67:1367
78. Kitano Y, Hood DW, Park K (1962) J Geophys Res 67:4873
79. Sohnel O, Mullin JW (1982) J Cryst Growth 60:239
80. Kitamura M, Konno H, Yasui A, Masuoka H (2002) J Cryst Growth 236:323
81. Heywood BR (1996) In: Mann S (ed) Biomimetic Materials Chemistry. VCH, Weinheim, p 143
82. Rajam S, Heywood BR, Walker JBA, Mann S, Davey RJ, Birchall JD (1991) J Chem Soc, Faraday Trans 87:727
83. Heywood BR, Mann S (1994) Chem Mater 6:311
84. Heywood BR, Mann S (1994) Adv Mater 6:9
85. Loste E, Diaz-Marti E, Zarbakhsh A, Meldrum F (2003) Langmuir 19:2830
86. Litvin AL, Samuelson LA, Charych DH, Spevak W, Kaplan DL (1995) J Phys Chem 99:12065
87. Berman A, Ahn DJ, Lio A, Salmeron M, Reichert A, Charych D (1995) Science 269:515
88. Ahn DJ, Berman A, Charych D (1996) J Phys Chem 100:12455
89. Champ S, Dickinson JA, Fallon PS, Heywood BR, Mascal M (2000) Angew Chem Int Ed 39:2716
90. Buijnsters PJJA, Donners JJJM, Hill SJ, Heywood BR, Nolte RJM, Zwanenburg B, Sommerdijk NAJM (2001) Langmuir 17:3623
91. Cavalli S, Popescu DC, Tellers EE, Vos MRJ, Pichon BP, Overhand M, Rapaport H, Sommerdijk NAJM, Kros A (2005) Angew Chem Int Ed 44:1
92. Litvin AL, Valiyaveettil S, Kaplan DL, Mann S (1997) Adv Mater 9:124
93. Volkmer D, Fricke M, Vollhardt D, Siegel S (2002) J Chem Soc Dalton Trans 4547
94. Volkmer D, Fricke M (2003) Z Anorg Allg Chem 629:2381
95. Volkmer D, Fricke M, Agena C, Mattay J (2002) CrystEngComm 4:288
96. Volkmer D, Fricke M, Gleiche M, Chi L (2005) Mater Sci Eng C 2:161
97. Lochhead MJ, Letellier SR, Vogel V (1997) J Phys Chem B 101:10821
98. Taylor DM (2000) Adv Colloid Interface Sci 87:183
99. Brockman H (1994) Chem Phys Lipids 73:57
100. Volkmer D, Fricke M, Agena C, Mattay J (2004) J Mater Chem 14:2249
101. Fricke M, Volkmer D, Krill CE III, Kellermann M, Hirsch A (2006) Cryst Growth Des 6:1120

102. Addadi L, Raz S, Weiner S (2003) Adv Mater 15:959
103. Olszta MJ, Odom DJ, Douglas EP, Gower LB (2003) Connect Tiss Res 44 Suppl 1:326
104. Weiss IM, Tuross N, Addadi L, Weiner S (2002) J Exp Zool 293:478
105. Politi Y, Arad T, Klein E, Weiner S, Addadi L (2004) Science 306:1161
106. Xu GF, Yao N, Aksay IA, Groves JT (1998) J Am Chem Soc 120:11977
107. DiMasi E, Patel VM, Sivakumar M, Olszta MJ, Yang YP, Gower LB (2002) Langmuir 18:8902
108. Nassif N, Pinna N, Gehrke N, Antonietti M, Jäger C, Cölfen H (2005) Proc Natl Acad Sci 102:12653
109. Duffy DM, Harding JH (2004) Langmuir 20:7630
110. Duffy DM, Harding JH (2004) Langmuir 20:7637
111. DiMasi E, Oltsza MJ, Patel VM, Gower L (2003) CrystEngComm 5:346
112. Volkmer D, Harms M, Gower L, Ziegler A (2005) Angew Chem Int Ed 44:639
113. BASF symposium on bioinspired materials for the chemical industry at ISIS in Strasbourg, France, 7–9 August 2006